STABILITY STUDY ON SHEAR FLOW AND VORTICES IN LATE BOUNDARY LAYER TRANSITION

by

JIE TANG

DISSERTATION

Submitted in partial fulfillment of the requirements

for the degree of Doctor of Philosophy at

The University of Texas at Arlington

August,2017

Arlington, Texas

Supervising Committee:

Chaoqun Liu, Supervising Professor

Hristo V. Kojouharov

Guojun Liao

Yue Liu

ACKNOWLEDGEMENTS

I would like to thank my supervising professor Dr. Chaoqun Liu for constantly motivating and encouraging me, and also for his invaluable advice during the five years of my doctoral studies. I wish to thank my academic advisors Dr. Guojun Liao, Dr. Hristo V.Kojouharov, Dr. Yue Liu and Dr. Jianzhong Su for their interest in my research and taking time to serve in my comprehensive committee and dissertation committee.

I would like to thank my co-workers Dr. Tian, Yong Yang, Huankun Fu, Yiqian Wang and many other friends at UTA, they helped me a lot in my research work and companied me in my time of living in the United States.

I wish to thank our math department, for the financial support in my doctoral program. I would also like to thank all the professors of our department who taught me in these years, especially Dr. Gaik Ambartsoumian, Dr. Vancliff, Dr. Sun-Mitchell and Dr. Hawkins, for whose classes I benefitted most.

Finally, I would like to express my deep gratitude to my parents, my uncle and all my family members. Without their love, I could not make this work success.

July 25, 2017

Abstract

STABILITY STUDY ON SHEAR FLOW AND DNS VORTICS GENERATION ON BOUNDARY LAYER TRANSITION

JIE TANG, Ph.D.

The University of Texas at Arlington, 2017

Supervising Professor: Chaoqun Liu

Turbulence is still an unsolved scientific problem, it has been regarded as “the most important unsolved problem of classical physics”. Dr. Liu proposed a new mechanism about turbulence generation and sustenance after decades of research on turbulence and transition. His new idea challenged the classical theorem in many aspects. One of them is the flow stability of transition. Dr. Liu believes that inside the flow field, shear (dominant in laminar) is very unstable while rotation (dominant in turbulence) is relative stable. This inherent property of flow creates the trend that non-vertical vorticity must transfer to vertical vorticity, and causes the occurrence of transition.

To verify this new idea, this dissertation analyses the linear stability on two-dimensional shear flow and quasi-rotation flow. 1) Chebyshev collocation spectral method is discussed to solve Orr–Sommerfeld equation, the famous eigenvalue function describing the linear modes of disturbance. Several typical parallel shear flows are tested as the basic-state flows in the equation. The instability of shear flow is demonstrated by the existence of positive eigenvalues associated with disturbance modes (eigenfunctions), i.e. the growth of these linear modes. 2) Quasi-rotation flow is considered under Cylindrical coordinate. An eigenvalue perturbation equation is derived to study the stability problem with symmetric flows. Shifted Chebyshev polynomial with Gauss collocation points is used to

solve the equation. To investigate the stability of vortices generation in real-world case, I tracked a ring-like vortex and a leg-like vortex over time from our Direct Numerical Simulation (DNS) data. The result shows that, with the generation over time, both ring-like vortex and leg-like vortex become more stable in the fact of decreasing positive eigenvalues.

Table of Contents

List of Illustrations

List of Tables

Chapter 1

INTRODUCTION

1.1 Introduction to boundary layer transition

In fluid dynamics, the process of a laminar flow becoming turbulent is a fundamental scientific problem, also known as laminar-turbulent transition. Laminar flow describes the fluid flows in parallel layers, with no disruption between the layers [1]. Turbulent flow is characterized by eddies or small packets of fluid particles which result in lateral mixing [2]. Laminar-turbulent transition is an extraordinarily complicated process which at present is still far from understood. Nevertheless, as the result of many decades of intensive research, classical comprehensive theories of physical mechanisms of the transition phenomenon have been established [3]–[5].

Boundary layer is a very important concept in transition theory. It is a thin layer of viscous fluid close to the solid surface of a wall in contact with a moving stream [6]. The flow velocity varies from zero at the wall up to approximate free stream velocity at the boundary. The fundamental concept of the boundary layer was suggested by L.Prandtl [7] in 1904. Modern research on fluid transition is most often studied in the context of boundary layers due to their ubiquity in real flows and their importance in many fluid-dynamic processes [8].

In a thin boundary layer, the velocity gradient is significant, and consequently the viscous shear stresses defined by

$$\tau = \mu \frac{du}{dy} \tag{1.1}$$

is large, where μ is the dynamic viscosity, $u = u(y)$ describes the profile of the boundary layer longitudinal velocity component, y is the normal-to-wall direction. In other words, in a thin boundary layer, laminar flow is dominant with shear layers.

Computation of the boundary layer parameters is based on the solution of equations obtained from the Navier–Stokes equations for viscous fluid motion. Navier-Stokes equation describes the conservation of mass, momentum, and of energy for the motion.

For boundary-layer flows, two main classes of transition are known [9]–[11] depend on the character of environmental disturbances. The first of them is usually observed when environmental disturbances are rather small. It is regarded as natural transition and has fundamental and practical importance in problems involving moving vehicles in air and water. The second class of transition, usually called bypass, is observed when high enough levels of environmental perturbations are presents.

Classical theory on natural transition can be described by four stages: receptivity, linear instability, non-linear growth and vortex breakdown as shown in Figure 1.1 [5].

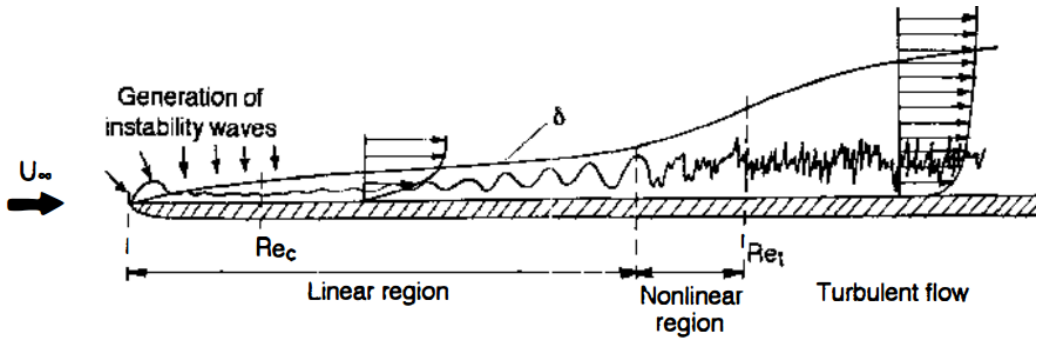

Figure 1-1 Qualitative sketch of the process of turbulence onset in a boundary layer. δ is the thickness of the boundary layer, Re represents the Reynolds number and U_∞ is the income free stream.

The initial stage of the natural transition process is known as the Receptivity phase and consists of the transformation of environmental disturbances into small perturbations (i.e. instability waves, usually called Tollmien-Schlichting waves) within the boundary layer. This aspect of the transition process was clearly formulated for the first time by Morkovin [10] in 1968. Many experimental and theoretical work of this process are appeared in the 1970s [12]–[16]. Details of the subsequent rapid development of investigations on receptivity can be found in numbers of books and review papers [17]–[21].

The second stage of transition corresponds to the linearly propagation of small-amplitude instability waves in the boundary. This stage is described by linear hydrodynamic stability theory, also called linear stability theory. Tollmien [22] started the research on linear stability theory in 1929. In the following century, it becomes the most developed branch of the transition problem with a lot of research achievements for two-dimensional and three-dimensional flows. For example, Schlichting [23], Lin [24], Herbert [25] and many others.

When the growth of linear instability waves reaches considerable values, the flow enters a phase of three-dimensional nonlinear growth, then the turbulent flow formed (so-called vortex breakdown). They are the last two stages. Although the region of nonlinear growth had been studied for more than half century, there are still many questions remaining [26]–[31]. For example, the mechanism of vortices generation and deformation, the formation of turbulence and turbulence coherent structure.

1.2 Liu's new theory on Boundary Layer transition

Dr. Liu proposed a new comprehensive mechanism about turbulence generation and sustenance in a boundary layer [32] after decades of research on turbulence and transition [33]–[49]. Many new observations are made and new mechanisms are revealed in late boundary layer transition [32] including:

(1) Mechanism of spanwise vorticity rollup.

(2) Mechanism of transfer from flow shear to rotation.

(3) Mechanism of spanwise vortex tube formation and role of the linear unstable modes.

(4) Mechanism of K -vortex root formation.

(5) Mechanism of first ring-like vortex formation.

(6) Mechanism of multiple vortex ring formation.

(7) Mechanism of second sweep formation.

(8) Mechanism of high share layer formation.

(9) Mechanism of positive spike formation.

(10) Mechanism of secondary and tertiary vortex formation.

(11) Mechanism of U-shaped vortex formation.

(12) Mechanism of small length vortices generation.

(13) Mechanism of multiple level high shear layer formation.

(14) Mechanism of energy transfer paths from the large length scale to the small ones.

(15) Mechanism of symmetry loss and flow chaos.

(16) Mechanism of thickening of turbulence boundary layer.

(17) Mechanism of high surface friction of turbulent flow.

This dissertation focuses on Dr. Liu's second proposal: Mechanism of transfer from flow shear to rotation. More precisely, the mechanism of transfer from non-vortical vorticity to vortical vorticity.

In Section 1.1, we introduced the laminar flow and turbulent flow. In boundary layer, laminar flow is dominant by shear because of large velocity gradient. Turbulent flow, consisted of eddies or small packets of fluid particles, is dominant by rotation. In classical stability theory, laminar is regarded as a stable state while turbulence is an unstable state with disorder, chaotic and random fluid layers. However, Dr. Liu has an opposite opinion, he believes that "Shear layer Instability" is the "mother of turbulence", rotation is more stable than shear when the Reynolds number is large enough. This inherent property of flow creates the trend that non-vertical vorticity must transfer to vertical vorticity, and causes the occurrence of transition.

Dr. Liu also pointed out the very commonly confusion of vorticity and vortex in fluid dynamics in his new paper [50], [51]. Vorticity has rigorous mathematical definition (curl of velocity), but no clear physical meaning. On the other hand, vortex has clear physical meaning (rotation) but no rigorous mathematical definition. For a long time, many researchers treat them as a same thing. Dr. Liu [50] gave the detailed DNS observations on the difference between vorticity and vortex, including:

(1) Vorticity tube is not vortex

(2) Vortex is not the congregation of vorticity.

(3) Vortex is never attached to the wall.

The classical description of "vortex breakdown" is also not accurate since rotation cannot break to pieces.

Based on Dr. Liu's discovery, some current stability analysis of vortices base on velocity-vorticity equation and vorticity profiles of base flow are questionable.

1.3 Propose of the Dissertation

To verify Dr. Liu's new idea, this dissertation first uses linear stability theory and Orr-Sommerfeld equation to analyze the instability of shear. Second, quasi-rotation velocity profiles extracted from lambda vortex of our DNS case are used to analyze the stability of rotation on boundary layer transition.

1.4 Organization of the Dissertation

This dissertation contains 7 chapters. Chapter I is the Introduction. Chapter 2 presents Navier-Stokes Equation and basic idea of linear stability theory. The numerical method: Chebyshev spectral method used in this dissertation is introduced in Chapter 3. Chapter 4 provides our DNS case set-up information and case validation. Chapter 5 studies the instability of 2D shear flow. Chapter 6 derives an eigenvalue perturbation equation with rotation flow under Cylindrical coordinate. Chapter 7 shows the numerical results of stability analysis on ring- and leg-like vortices.

Chapter 2

NAVIER-STOKES EQUATIONS AND LINEAR STABILITY THEORY

2.1 Conservation Laws and the Equations

The motion of a fluid can be described by the conservation of mass, momentum, and of energy for an arbitrary small control volume.

Consider a closed surface S whose position is fixed with relation to the coordinate axes and encloses a volume V completed filled with fluid. Given the density of the fluid ρ, the momentum $\rho\boldsymbol{u}$, the total energy E at a position x and at time t, the Navier-Stokes equations can be derived as follows from the conservation laws of mass, momentum and energy:

$$\frac{\partial \rho}{\partial t} + \nabla \cdot (\rho \boldsymbol{u}) = 0, \tag{2.1}$$

$$\frac{\partial (\rho \boldsymbol{u})}{\partial t} + \nabla \cdot (\rho \boldsymbol{u} \otimes \boldsymbol{u}) = \nabla \cdot \sigma, \tag{2.2}$$

$$\frac{\partial (\rho E)}{\partial t} + \nabla \cdot (\rho E)\boldsymbol{u} - \nabla \cdot (k \nabla T) - \nabla \cdot (\sigma \cdot \boldsymbol{u}) = 0, \tag{2.3}$$

with

$$E = e + \frac{\boldsymbol{u} \cdot \boldsymbol{u}}{2}, \tag{2.4}$$

and

$$\sigma = -\left[\rho + \frac{2}{3}\mu(\nabla \cdot \boldsymbol{u})\right]\boldsymbol{I} + \mu[\nabla \boldsymbol{u} + (\nabla \boldsymbol{u})^T]. \tag{2.5}$$

Here, σ is the internal shear stress, e is the internal energy per unit mass of the fluid, p denotes the pressure, T represents the temperature, k is the thermal conductivity and μ is the dynamic viscosity. Stokes [52] assumption, linear relation between the stress and the rate of strain of the fluid, is used in obtaining the Equation (2.5).

In three dimensions, the system above contains five equations (the conservation of momentum equation becomes three separate equations). Two extra equations are needed to solve the system for the unknown variable $\rho, \boldsymbol{u}, p, E$ and T. These equations are the equation of state, for a thermally perfect gas,

$$p = \rho RT, \tag{2.6}$$

where R is a gas constant, and the equation for internal energy,

$$e = c_V T. \tag{2.7}$$

2.2 Non-Dimensional Form of the governing equation

Equations (2.1) - (2.6) can be reduced to a non-dimensional form. This can be achieved by dividing each variable by an appropriate dimensional reference parameter. Those reference parameters are defined as follows, where ∞ indicates incoming or free stream values:

L is the characteristic length;

V_∞ is the speed;

ρ_∞ is the density;

p_∞ is the pressure;

T_∞ is the temperature;

μ_∞ is the dynamic viscosity;

k_∞ is the thermal conductivity.

With these reference parameters, the non-dimensional variables are given by

$$t = \frac{t^*}{L/V_\infty}, \boldsymbol{x} = \frac{\boldsymbol{x}^*}{L}, \boldsymbol{u} = \frac{\boldsymbol{u}^*}{V_\infty}, p = \frac{p^*}{\rho_\infty V_\infty^2}, \boldsymbol{\sigma} = \frac{\boldsymbol{\sigma}^*}{\rho_\infty V_\infty^2} \tag{2.8}$$

where $*$ represents the dimensional variables.

Rewrite the equations in the section 2.1 in non-dimensional form, we can obtain:

$$\frac{\partial \rho}{\partial t} + \nabla \cdot (\rho \boldsymbol{u}) = 0 \tag{2.9}$$

$$\frac{\partial (\rho u)}{\partial t} + [\nabla \cdot (\rho \boldsymbol{u} \otimes \boldsymbol{u})] = \nabla \cdot \sigma \tag{2.10}$$

$$\frac{\partial (\rho E)}{\partial t} + \nabla \cdot (\rho E)\boldsymbol{u} - \frac{\gamma}{RePr} \nabla \cdot (\nabla T) - \gamma(\gamma - 1) M_\infty^2 \nabla \cdot (\sigma \cdot \boldsymbol{u}) = 0 \tag{2.11}$$

$$\sigma = -\left[p + \frac{2}{3}\frac{1}{Re}\mu(T)(\nabla \cdot \boldsymbol{u})\right]\boldsymbol{I} + \frac{1}{Re}\mu(T)[\nabla \boldsymbol{u} + (\nabla \boldsymbol{u})^T] \tag{2.12}$$

$$p = \frac{1}{\gamma M_\infty^2}\rho T \tag{2.13}$$

The Reynolds number is defined as

$$Re = \frac{\rho_\infty V_\infty L}{\mu_\infty} \tag{2.14}$$

while the Prandtl number evaluated at the reference conditions is given by

$$Pr = \frac{c_p \mu_\infty}{k_\infty} \approx 0.72 \tag{2.15}$$

And the Mach number is defined as

$$M_\infty = \frac{V_\infty}{\sqrt{\gamma R T_\infty}} \tag{2.16}$$

The dynamic viscosities coefficient is given by Sutherland's equation:

$$\mu = T^{\frac{2}{3}}\frac{1 + C}{T + C}\,, C = \frac{110.4}{T_\infty} \tag{2.17}$$

2.3 Introduction to Linear stability theory

The basic idea behind linear stability theory is to superpose small disturbances on the local, undisturbed flow state (termed the "basic state") and determine whether these perturbations grow or decay. If all perturbations decay, then the flow is termed stable, vice-versa. The analysis is performed locally by linearizing the complete unsteady Navier-Stokes equations (see section 2.1 and 2.2) about the basic state.

Designate (x, y, z) as the streamwise, normal-to-the-wall and spanwise coordinates. The stability equations, also called Orr-Sommerfeld equations are obtained by superposing small disturbances q' onto the basic state, which gives total flow quantities q of the form

$$Q(x, y, z, t) = Q(y) + q'(x, y, z, t) \tag{2.18}$$

The quantities q and Q separately satisfy the complete Navier-Stokes equations and therefore separately represent real flows, whereas the disturbance quantities q' do not. When the basic-state solution is dropped from the equations describing q, the equations in terms of the disturbance quantities q' result. These equations are further simplified by making the approximation that products of disturbance quantities are neglected, i.e. the disturbance equations are linearized.

For example, the disturbance equations are linear and if the coefficients are functions of y only. This suggests a solution for q' in terms of separation of variables using normal modes (i.e. exponential solutions in terms of the independent variables x, z, and t) to reduce the disturbance equations to ordinary differential equations. Therefore, the normal-mode approach is generalized as:

$$q' = q_0(y)\, exp(i\Theta) + c.c. \tag{2.19}$$

where c.c. stands for complex conjugate and $\Theta(x, y, t)$ is the phase function

$$\frac{\partial \Theta}{\partial x} = \alpha, \frac{\partial \Theta}{\partial z} = \beta, \frac{\partial \Theta}{\partial t} = -\omega \tag{2.20}$$

Here, α is the streamwise wavenumber, β is the spanwise wavenumber, and ω is the frequency. The amplitude function $q(y)$ is complex and q' is real because the Navier-Stokes equations are real.

The system constitutes an eigenvalue problem for the eigenvector $q(y)$. For a well-posed eigenvalue problem such as plane Poiseuille flow, there is an infinite set of discrete eigenvalues and a corresponding infinite discrete set of eigenfunctions. For boundary layers, there is a finite discrete set of eigenvalues as well as a continuous spectrum. The eigenfunctions are called modes and form a basis for an arbitrary disturbance profile. For incompressible streamwise instabilities, the least stable mode is called the first mode and because there is no more than one unstable mode, not much attention is paid to higher modes. For some flows (e.g. centrifugal instabilities), more than one mode can be unstable.

Disturbances can be classified with respect to spatial amplification, temporal amplification, and spatial and temporal amplification. In spatial theory, ω is assumed to be real, while α and β are assumed to be complex. Their real parts, α_r and β_r, represent the physical wavenumbers of the disturbances, while their imaginary parts, α_i and β_i, represent the growth (or decay) rates in the x and y directions, respectively. In temporal theory, α and β are assumed to be real and ω is assumed to be complex. For both temporal and spatial amplification, ω, α and β are all assumed to be complex.

For temporal stability, the dispersion relation:

$$\omega = f(\beta, \alpha, Re) \tag{2.21}$$

yields the unique pair (ω_r, ω_i) when β, α and Reynolds number Re are specified. Because ω appears linearly in the stability equations, much of the early work of transition focused on this case. Therefore, this thesis discusses the temporal stability analysis.

Chapter 3

CHEBYSHEV SPECTRAL METHODS

3.1 Introduction to Spectral Methods

Spectral methods are an important development of the class of discretization schemes for differential equations, known generically as the method of weighted residuals (MWR) [53]. The key elements of MWR are the trial functions (also called the expansion or approximating functions) and the test functions (also known as weight functions).

The general scheme of MWR is first to get a truncated series expansion of the solution by the trial functions. Then the residual can be produced by using the truncated expansion in the differential equation. Last, a desired truncated series expansion is achieved by minimizing the residual with respect to a suitable norm, defined as an orthogonality condition with respect to each of the test functions.

The choice of trial functions is one of the features which distinguish spectral methods from finite-element and finite-difference method. The trial functions for spectral methods are infinitely differentiable global functions, while the trial functions for finite-element method or finite-difference method are specified locally in each element or cell. The most frequently used trial functions are trigonometric polynomials, Chebyshev polynomials and Legendre polynomials.

The choice of test functions leads to three most commonly used spectral methods schemes: Galerkin, collocation, and tau. In the Galerkin approach, the test functions are the same as the trial functions. It requires that the integral of the residual times each test function to be zero. In the collocation approach the test functions are translated Dirac Delta functions centered at special points, namely collocation points. This approach requires the residual to be zero at the collocation points. The tau approach is similar to the Galerkin approach with a supplementary set of equations is used to apply the boundary conditions.

3.2 Chebyshev polynomials of first kind

The Fourier method is the most commonly used spectral method with trigonometric polynomials as trial functions. It is appropriate for periodic problems, but is not adapted to non-periodic problems because of the existence of the Gibbs phenomenon at the boundaries. In this dissertation, the cases are all non-periodic problems, so better-suited trial functions like Chebyshev polynomials constitute a proper alternative to the Fourier method. Especially in a bounded domain, the use of Chebyshev polynomials has been advantageous. The stability calculations shown in this dissertation have been obtained by Chebyshev discretization of the Cartesian and Cylindrical coordinates.

Let us first consider the definition and some properties of the Chebyshev polynomials of the first kind [54].

Definition (Chebyshev polynomial of the first kind $T_n(x)$). The Chebyshev polynomial of the first kind of order n is defined as follows:

$$\mathrm{T_n}(x) = \cos[n\cos^{-1}(x)], \qquad x \in [-1,1], \qquad n = 0,1,2,\cdots \tag{3.1}$$

From this definition, the following property is evident by setting $\mathrm{x} = \cos\theta$:

$$\mathrm{T_n}(\cos\theta) = \cos(n\theta), \qquad \theta \in [0,\pi], \qquad n = 0,1,2,\cdots \tag{3.2}$$

Properties of the Chebyshev polynomials $\mathrm{T_n}(x)$

The polynomials $\mathrm{T_n}(x), n \geq 1$, satisfy the following properties, which follow straightforwardly from (3.1):

1) The Chebyshev polynomials $\mathrm{T_n}(x)$ satisfy the following three-term recurrence relations:

$$\mathrm{T_{n+1}}(x) = 2xT_n(x) - T_{n-1}(x), \qquad n = 1,2,3,\cdots, \tag{3.3}$$

with starting values $\mathrm{T_0}(x) = 1, \mathrm{T_1}(x) = x$.

Explicit expressions for the first seven Chebyshev polynomials are

$$T_o(x) = 1,$$

$$T_1(x) = x,$$

$$T_2(x) = 2x^2 - 1,$$

$$T_3(x) = 4x^3 - 3x,$$

$$T_4(x) = 8x^4 - 8x^2 + 1,$$

$$T_5(x) = 16x^5 - 20x^3 + 5x,$$

$$T_6(x) = 32x^6 - 48x^4 + 18x - 1. \qquad (3.4)$$

The graphs of these Chebyshev polynomials are plotted in Figure 3-1.

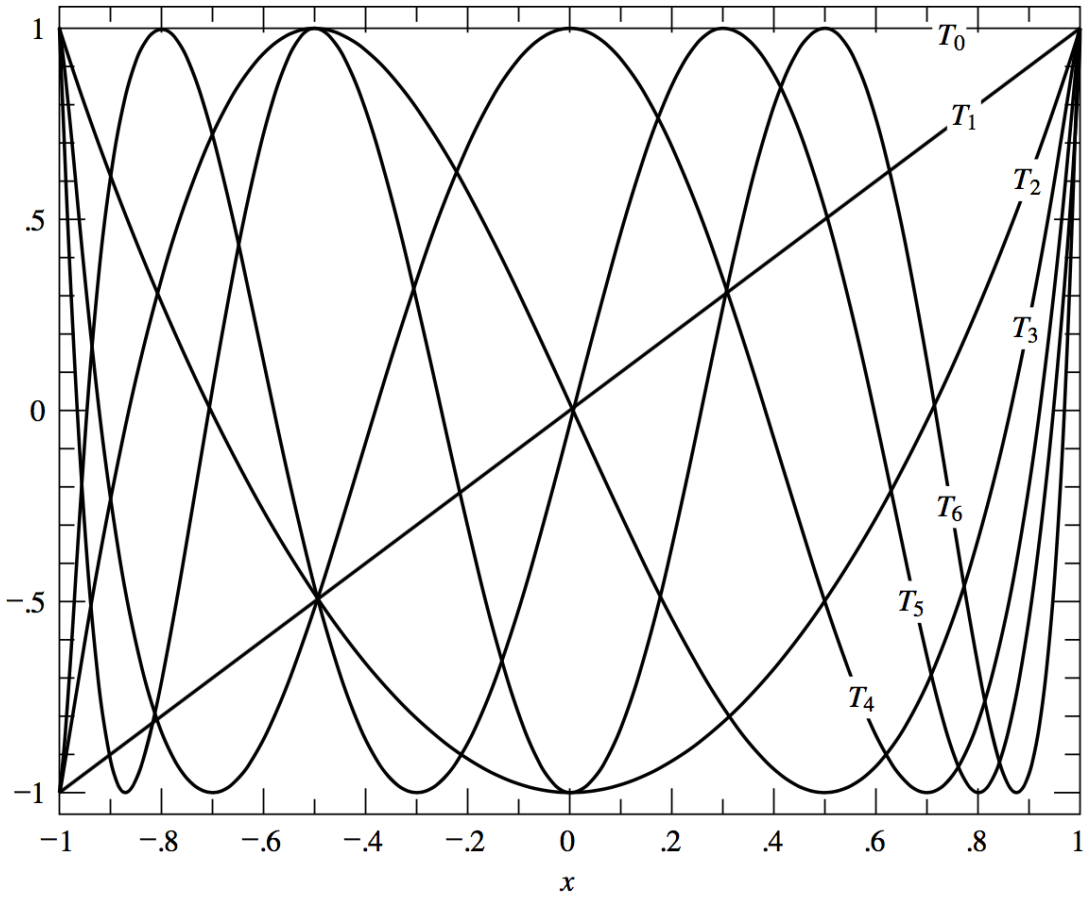

Figure 3-1 Chebyshev polynomials $T_0(x)$ through $T_6(x)$

2) The leading coefficient (of x^n) in $T_n(x)$ is 2^{n-1} and $T_n(-x) = (-1)^n T_n(x)$.

3) $T_n(x)$ has n zeros which lie in the interval $(-1,1)$. They are given by

$$x_k = \cos\left(\frac{2k+1}{2n}\pi\right), \qquad k = 0,1,\cdots,n-1. \tag{3.5}$$

These points are called Chebyshev nodes or Gauss points.

$T_n(x)$ has $n+1$ extrema in the interval $[-1,1]$ and they are given by

$$x'_k = \cos\frac{k\pi}{n}, \qquad k = 0,1,\cdots,n. \tag{3.6}$$

At these points, the values of the polynomials are $T_n(x'_k) = (-1)^k$.

They are called Gauss-Lobatto points.

4) The differentiation of T_n gives

$$T'_n(x) = \frac{d}{d\theta}(cosn\theta)\frac{d\theta}{dx} = n\frac{sink\theta}{sin\theta}, \qquad n = 0,1,2,\cdots. \tag{3.7}$$

By the application of trigonometrical formulas, the recurrence relation on the derivative is:

$$\frac{T'_{n+1}(x)}{n+1} - \frac{T'_{n-1}(x)}{n-1} = 2T_n(x), \qquad n = 1,2,3,\cdots, \tag{3.8}$$

with $T'_0(x) = 0, T'_1(x) = 1$.

5) Orthogonality relation

$$\int_{-1}^{1} T_r(x)T_s(x)(1-x^2)^{-\frac{1}{2}}dx = N_r\delta_{rs}, \tag{3.9}$$

With $N_0 = \pi$ and $N_r = \frac{1}{2}\pi$ if $r \neq 0$.

This property means that the set of Chebyshev polynomials $\{T_n(x)\}$ is an orthogonal set with respect to the weight function $w(x) = (1-x^2)^{-1/2}$ in the interval (-1,1).

6) Discrete orthogonality relation

a) With the zeros of $T_{n+1}(x)$ as nodes (Chebyshev nodes): Let $n > 0$, $r, s \leq$

n, and $x_j = \cos\left(\frac{\left(j+\frac{1}{2}\right)\pi}{n+1}\right)$. Then,

$$\sum_{j=0}^{n} T_r(x_j)T_s(x_j) = K_r\delta_{rs}\,, \tag{3.10}$$

where $K_0 = n+1$ and $K_r = \frac{1}{2}(n+1)$ when $1 \le r \le n$.

b) With the extrema of $T_n(x)$ as nodes (Gauss-Lobatto points): Let $n > 0$, $r, s \le n$, and $x_j = \cos\left(\frac{j\pi}{n}\right)$. Then

$$\sum_{j=0}^{n}{}'' T_r(x_j)T_s(x_j) = K_r\delta_{rs}\,, \tag{3.11}$$

where $K_0 = K_n = n$ and $K_r = \frac{1}{2}n$ when $1 \le r \le n-1$.

The double prime indicates that the terms with suffixes $j = 0$ and $j = n$ are to be halved.

3.3 Chebyshev collocation approach

Chebyshev collocation (i.e. interpolation) is a useful technique to approximate a given function. The commonly used collocation points are the Gauss-Lobatto points. The advantage of Gauss-Lobatto points is that both the boundary points are included.

Consider the Chebyshev approximation of the function $u(x)$ defined for $x \in [-1,1]$:

$$u_N(x) = \sum_{n=0}^{N} a_n T_n(x)\,. \tag{3.12}$$

The technique consists of setting to zero the residual $R_N = u - u_N$ at the collocation points $x_i = \frac{cos\pi i}{N}, i = 0, \cdots, N$, let

$$u(x_i) = u_N(x_i) = \sum_{n=0}^{N} a_n T_n(x_i)\,, \qquad i = 0 \cdots, N. \tag{3.13}$$

When discretizing ordinary or partial differential equations, derivatives of the solution are need as well. These derivatives have to be expressed in terms of Chebyshev polynomials and the following recurrence relation between Chebyshev polynomials are their derivatives is used.

$$\mathrm{T}_0^{(\mathrm{k})}(x_i) = 0,$$

$$\mathrm{T}_1^{(k)}(x_i) = \mathrm{T}_0^{(k-1)}(x_i),$$

$$\mathrm{T}_2^{(k)}(x_i) = 4\mathrm{T}_1^{(k-1)}(x_i),$$

$$\mathrm{T}_n^{(k)}(x_i) = 2nT_{n-1}^{(k-1)}(x_i) + \frac{n}{n-2}T_{n-2}^{(k)}(x_i), \qquad n = 3,4,\cdots. \tag{3.14}$$

with the superscript $\mathrm{k} \geq 1$ denoting the order of differentiation.

3.4 Convergence of Chebyshev spectral method

An important difference between finite-difference approximations to the eigenvalues and eigenfunctions equation like Orr-Sommerfeld equation and the Chebyshev approximations is their order of accuracy. Finite-difference approximations give only a finite order of accuracy in the sense that errors behave like $(\Delta \mathrm{x})^{\mathrm{p}}$ for some finite p when the grid scale $\Delta \mathrm{x}$ approaches zero. On the other hand, if the basic-state velocity profile $\bar{\mathrm{u}}(\mathrm{y})$ is infinitely differentiable, the Chebyshev polynomial approximations used here are of infinite order in the sense that error decrease more rapidly than any power of $1/\mathrm{N}$ as $\mathrm{N} \to \infty$.

The latter statement is verified by Orszag [55]. If $\bar{\mathrm{u}}(\mathrm{y})$ is infinitely differentiable, all the eigenfunction $\mathrm{v}(\mathrm{y})$ of the Orr-Sommerfeld equation are infinitely differentiable for $\mathrm{y} \in [-1,1]$ (with one-sided derivatives at the end-points). $\mathrm{T}_\mathrm{n}(y)$ denotes the nth-degree Chebyshev polynomial of the first kind. Recall equation 3.2, defined $\mathrm{y} = \cos\theta$:

$$\mathrm{T}_\mathrm{n}(cos\theta) = cosn\theta$$

For all non-negative integers n. It is possible to expand $\mathrm{v}(\mathrm{y})$ in the interval $\mathrm{y} \in [-1,1]$ as

$$\mathrm{v}(\mathrm{y}) = \sum_{n=0}^{\infty} a_n T_n(y) \tag{3.15}$$

where

$$a_n = \frac{2}{\pi c_n} \int_{-1}^{1} v(y) T_n(y) (1 - y^2)^{-\frac{1}{2}} dy \tag{3.16}$$

with $\mathrm{c_o} = 2, c_n = 1$. The rapidity of convergence of equation (3.3) for $|\mathrm{y}| \leq 1$ is easily demonstrated by observing that

$$\mathrm{f}(\theta) = \mathrm{v}(\cos\theta) \tag{3.17}$$

Is an infinitely differentiable, even, periodic function of θ.

Consequently, the theory of Fourier series ensures that $\mathrm{f}(\theta)$ possesses a Fourier cosine expansion

$$\mathrm{f}(\theta) = \sum_{n=0}^{\infty} a_n cosn\theta \tag{3.18}$$

with the property that the error after N terms decreases more rapidly than any power of $1/\mathrm{N}$ as $\mathrm{N} \to \infty$. The expansion (3.6) is precisely equation (3.3) for $\mathrm{y} = \cos\theta$.

Moreover, the error associated with the Chebyshev approximation is $\mathrm{O}(1/\mathrm{N}^{\mathrm{m}})$ where N refers to the truncation and m is connected to the number of continuous derivatives (if finite) of function under consideration.

3.5 Advantages of Chebyshev nodes

In polynomial interpolation, Chebyshev nodes provide the resulting interpolation polynomial minimizes the effect of Runge's phenomenon.

Given a function $f \in \mathcal{C}^N[-1,1]$ and Chebyshev nodes $y_0, \dots, y_{N-1}$, for each $y \in [-1,1]$, a number $\xi(y)$ exists in $(-1,1)$ with

$$f(y) - P_{N-1}(y) = \frac{f^{(N)}(\xi(y))}{N!} \prod_{j=0}^{N-1} (y - y_j) \tag{3.19}$$

where $P_{N-1}(y)$ is the Lagrange interpolating polynomial.

Notice that $\prod_{j=0}^{N-1}(y - y_j)$ is the monic Chebyshev polynomial, that is,

$$\prod_{j=0}^{N-1} (y - y_j) = \frac{T_N(y)}{2^{N-1}}. \tag{3.20}$$

Recall $T_N(y) = \cos(n \cos^{-1}(y))$, we have

$$\left| \prod_{j=0}^{N-1} (y - y_j) \right| \leq \frac{1}{2^{N-1}} \tag{3.21}$$

Then

$$\max_{y \in [-1,1]} |f(y) - P_{N-1}(y)| \leq \frac{1}{2^{N-1} N!} \max_{y \in [-1,1]} \left| f^{(N)}(y) \right| \tag{3.22}$$

From Equation (3.22), it is obviously that with high order polynomial interpolation, the error is very small.

Chapter 4

DIRECT NUMERICAL SIMULATION (DNS) CASE SET UP AND CODE VALIDATION

To investigate the linear stability problem of vortices in real-world case, our high order DNS with near 60 million grid points and about 400,000 time steps are used to visualize and track the generation of vortices on boundary layer flow transition.

4.1 Case Set-up

The computation domain of our DNS case is shown in Figure 4-1. The mesh includes $1920 \times 128 \times 241$ points in streamwise (x), spanwise (y), and normal-to-wall (z) directions respectively. The grid is uniform in the streamwise and spanwise directions, while stretched in the normal direction. The first grid interval is carefully chosen to make sure the grid is fine enough to capture all the small scales ($Z^+ = 0.43$).

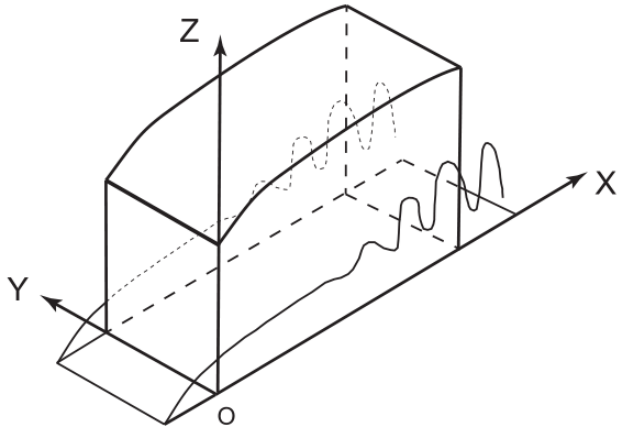

Figure 4-1 Computational Domain

The parallel computation is accomplished through the Message Passing Interface (MPI) together with the streamwise direction domain decomposition (shown in Figure 4-2). The flow conditions, including Reynolds number, Mach number, etc. are listed in Table 1.

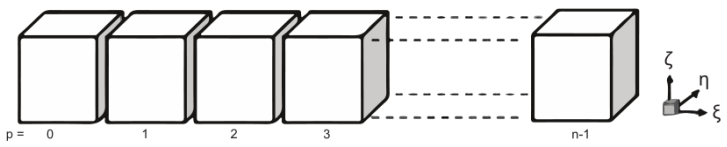

Figure 4-2 Domain decomposition for MPI

Table 4-1 Flow parameters

M_∞	Re	x_{in}	Lx
0.5	1000	$300.79\delta_{in}$	$798.03\delta_{in}$
Ly	Lz_{in}	T_w	T_∞
$22\delta_{in}$	$40\delta_{in}$	273.15K	273.15K

where

M_∞ = Mach number

Re = Reynolds number, define as $\frac{\rho_\infty U_\infty \delta_{in}}{\mu_\infty}$

δ_{in} = inflow displacement thickness

T_w = wall temperature

T_∞ = free stream temperature

Lz_{in} = height at inflow boundary

Lz_{out} = height at outflow boundary

Lx= length of computational domain along x direction

Ly= length of computational domain along y direction

x_{in} = distance between leading edge of flat plate and upstream boundary of computational domain

4.2 Governing equation in generalized curvilinear coordinates

The governing equations with three-dimensional compressible flow in Cartesian coordinates are shown in chapter 2. In this section, we give the expansion in Curvilinear Coordinates(ξ, η, ζ).

Equations (2.9)-(2.11) can be rewritten by a vector form:

$$\frac{\partial \mathrm{Q}}{\partial \mathrm{t}} + \frac{\partial E}{\partial x} + \frac{\partial F}{\partial y} + \frac{\partial G}{\partial z} = \frac{\partial E_v}{\partial x} + \frac{\partial F_v}{\partial y} + \frac{\partial G_v}{\partial z} \tag{4.1}$$

where

$$\mathrm{Q} = \begin{bmatrix} \rho \\ \rho u \\ \rho v \\ \rho w \\ e \end{bmatrix} \quad E = \begin{bmatrix} \rho u \\ \rho u^2 + p \\ \rho uv \\ \rho uw \\ (e+p)u \end{bmatrix} \quad F = \begin{bmatrix} \rho v \\ \rho vu \\ \rho v^2 + p \\ \rho vw \\ (e+p)v \end{bmatrix} \quad G = \begin{bmatrix} \rho w \\ \rho wu \\ \rho wv \\ \rho w^2 + p \\ (e+p)w \end{bmatrix} \tag{4.2}$$

$$\mathrm{E_v} = \frac{1}{Re} \begin{bmatrix} 0 \\ \tau_{xx} \\ \tau_{xy} \\ \tau_{xz} \\ u\tau_{xx} + v\tau_{xy} + w\tau_{xz} + q_x \end{bmatrix} \tag{4.3}$$

$$\mathrm{F_v} = \frac{1}{Re} \begin{bmatrix} 0 \\ \tau_{yx} \\ \tau_{yy} \\ \tau_{yz} \\ u\tau_{yx} + v\tau_{yy} + w\tau_{yz} + q_y \end{bmatrix} \tag{4.4}$$

$$\mathrm{G_v} = \frac{1}{Re} \begin{bmatrix} 0 \\ \tau_{zx} \\ \tau_{zy} \\ \tau_{zz} \\ u\tau_{zx} + v\tau_{zy} + w\tau_{zz} + q_z \end{bmatrix} \tag{4.5}$$

$$\mathrm{q_x} = \frac{\mu}{(\gamma-1)M_\infty^2 Pr} \frac{\partial T}{\partial x} \tag{4.6}$$

$$\mathrm{q_y} = \frac{\mu}{(\gamma-1)M_\infty^2 Pr} \frac{\partial T}{\partial y} \tag{4.7}$$

$$\mathrm{q_z} = \frac{\mu}{(\gamma-1)M_\infty^2 Pr} \frac{\partial T}{\partial z} \tag{4.8}$$

$$\mathrm{p} = \frac{1}{\gamma \mathrm{M}_{\infty}^{2}} \rho T \tag{4.9}$$

$$\tau = \mu \begin{bmatrix} \frac{4}{3}\frac{\partial u}{\partial x} - \frac{2}{3}\left(\frac{\partial v}{\partial y} + \frac{\partial w}{\partial z}\right) & \frac{\partial u}{\partial y} + \frac{\partial v}{\partial x} & \frac{\partial u}{\partial z} + \frac{\partial w}{\partial x} \\ \frac{\partial u}{\partial y} + \frac{\partial v}{\partial x} & \frac{4}{3}\frac{\partial u}{\partial x} - \frac{2}{3}\left(\frac{\partial w}{\partial z} + \frac{\partial u}{\partial x}\right) & \frac{\partial v}{\partial z} + \frac{\partial w}{\partial y} \\ \frac{\partial u}{\partial z} + \frac{\partial w}{\partial x} & \frac{\partial v}{\partial z} + \frac{\partial w}{\partial y} & \frac{4}{3}\frac{\partial u}{\partial x} - \frac{2}{3}\left(\frac{\partial u}{\partial x} + \frac{\partial v}{\partial y}\right) \end{bmatrix} \tag{4.10}$$

Assume that the position frame of reference is fixed in time, i.e. the generalized coordinates do not change with time. Then, we can define the curvilinear coordinates in relation to the Cartesian coordinates as

$$\begin{cases} \xi = \xi(x, y, z) \\ \eta = \eta(x, y, z) \\ \zeta = \zeta(x, y, z) \end{cases} \tag{4.11}$$

Thus, The Navier-Stokes equations can be transformed to the system using generalized coordinates:

$$\frac{\partial \widehat{\mathrm{Q}}}{\partial \tau} + \frac{\partial \hat{E}}{\partial \xi} + \frac{\partial \hat{F}}{\partial \eta} + \frac{\partial \hat{G}}{\partial \zeta} = \frac{\partial \hat{E}_{v}}{\partial \xi} + \frac{\partial \hat{F}_{v}}{\partial \eta} + \frac{\partial \hat{G}_{v}}{\partial \zeta} \tag{4.12}$$

with $\widehat{\mathrm{Q}} = J^{-1}Q$ and

$$\widehat{\mathrm{E}} = J^{-1}\left(\xi_x E + \xi_y F + \xi_z G\right) \tag{4.13}$$

$$\widehat{\mathrm{F}} = J^{-1}\left(\eta_x E + \eta_y F + \eta_z G\right) \tag{4.14}$$

$$\hat{G} = J^{-1}\left(\zeta_x E + \zeta_y F + \zeta_z G\right) \tag{4.15}$$

$$\hat{\mathrm{E}}_v = J^{-1}\left(\xi_x E_v + \xi_y F_v + \xi_z G_v\right) \tag{4.16}$$

$$\hat{\mathrm{F}}_v = J^{-1}\left(\eta_x E_v + \eta_y F_v + \eta_z G_v\right) \tag{4.17}$$

$$\hat{G}_v = J^{-1}\left(\zeta_x E_v + \zeta_y F_v + \zeta_z G_v\right) \tag{4.18}$$

$$\mathrm{J}^{-1} = \det\left(\frac{\partial(x,y,z)}{\partial(\xi,\eta,\zeta)}\right) \tag{4.19}$$

4.3 Numerical Methods

A sixth order compact scheme [56] is used for the spatial discretization in the streamwise and normal-to-wall directions. The scheme is used for internal points $\mathrm{j} = 3,\cdots,\mathrm{N}-2$ as follows:

$$\frac{1}{3}f'_{j-1} + \mathrm{f}'_{\mathrm{j}} + \frac{1}{3}f'_{j+1} = \frac{1}{\mathrm{h}}\left(-\frac{1}{36}f_{j-2} - \frac{7}{9}f_{j-1} + \frac{7}{9}f_{j+1} + \frac{1}{36}f_{j+2}\right) + O(h^6) \tag{4.20}$$

where f'_{j} is the first derivative at the internal point j. The fourth order compact scheme is used at point $\mathrm{j} = 2, \mathrm{N}-1$, and the third order one-sided compact scheme is used at the boundary points $\mathrm{j} = 1, \mathrm{N}$.

In the spanwise direction, the pseudo-spectral method is used for the periodical conditions. To eliminate the spurious numerical oscillations caused by central difference schemes, a high-order spatial scheme is used instead of artificial dissipation. An implicit sixth-order compact scheme for space filtering is applied to the primitive variables $\mathrm{u}, \mathrm{v}, \mathrm{w}, \rho, \mathrm{p}$ after a specified number of time steps.

The governing equations are solved explicitly by a 3rd order TVD Runge-Kutta scheme for time marching:

$$\mathrm{Q}^{(0)} = Q^n$$

$$\mathrm{Q}^{(1)} = Q^{(0)} + \Delta t R^{(0)}$$

$$\mathrm{Q}^{(2)} = \frac{3}{4}Q^{(0)} + \frac{1}{4}Q^{(1)} + \frac{1}{4}\Delta t R^{(1)}$$

$$\mathrm{Q}^{n+1} = \frac{1}{4}Q^{(0)} + \frac{2}{3}Q^{(2)} + \frac{2}{3}\Delta t R^{(2)} \qquad (4.21)$$

$\mathrm{CFL} \leq 1$ is required to ensure the stability.

The adiabatic and the non-slipping conditions are enforced at the wall boundary on the flat plate. On the far field and the outflow boundaries, the non-reflecting boundary conditions are applied.

Blasius solution with enforced disturbance is introduced into inlet as a laminar base inflow. The disturbance includes a two-dimensional T-S wave and a pair of conjugate three-dimensional T-S waves. The inflow has a form:

$$\mathrm{q} = \mathrm{q}_{\mathrm{lam}} + A_{2d} q'_{2d} e^{i(\alpha_{2d} x - \omega t)} + A_{3d} q'_{3d} e^{i(\alpha_{3d} x \pm \beta y - \omega t)}$$

with q represents the vector (u,v,w,p,T), $\mathrm{q}_{\mathrm{lam}}$ is the Blasius solution for a two-dimensional laminar flat plat boundary layer. The streamwise wavenumber, spanwise wavenumber, frequency and amplitude are given respectively as follows:

$$\alpha_{2\mathrm{d}} = 0.29919 - i5.09586 \times 10^{-3}$$

$$\beta = \pm 0.5712$$

$$\omega = 0.114027$$

$$\mathrm{A}_{2\mathrm{d}} = 0.03$$

$$\mathrm{A}_{3\mathrm{d}} = 0.01$$

The T-S wave parameters are obtained by solving the compressible boundary layer stability equations.

4.4 Code Validation

The code ”DNSUTA” was developed at the University of Texas at Arlington and carefully validated by NASA Langley and UTA researchers [40], [57]. Only a short description of the validation would be addressed here and readers are encouraged to refer to these papers for details. A more detailed comparison is also reported in [32].

4.4.1 Velocity profiles and grid convergence

Time and spanwise-averaged streamwise velocity profiles for two different streamwise locations in two different grids levels $960 \times 64 \times 121$ and $1920 \times 128 \times 241$ are shown respectively in Figure 4-3 (a) and Figure 4-3 (b). The inflow velocity profiles at $\mathrm{x} = 300.79\delta_{\mathrm{in}}$ is a typical laminar boundary layer velocity profile. And the mean velocity profile at $\mathrm{x} = 632.33\delta_{in}$ approaches a turbulent flow velocity profile (Log Law). This comparison shows that the grid convergence has been realized and the simulation from laminar flow to turbulence has also been achieved.

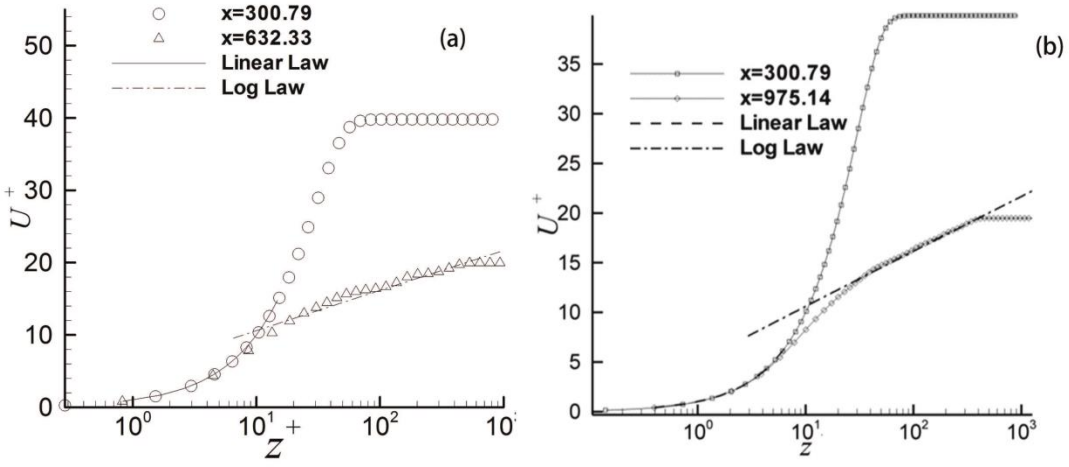

Figure 4-3 Time- and spanwise-averaged velocity profile in two grid levels

4.4.2 Comparison with experiment

Utilizing the λ_2-eigenvalue method proposed by Jeong and Hussain [58], the vortical structures during transition is shown in Figure 4-4. The formation of ring-like vortices chains is consistent with the experimental work by Lee and Li [59] as shown in Figure 4-5.

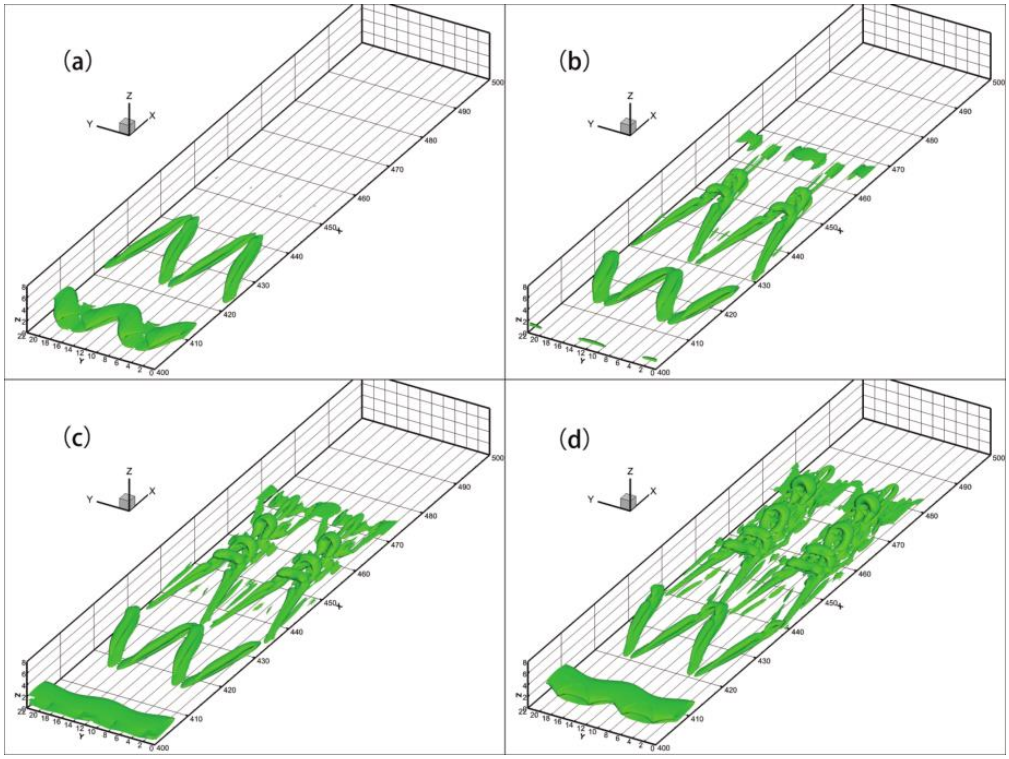

Figure 4-4 Evolution of vortical structures during transition

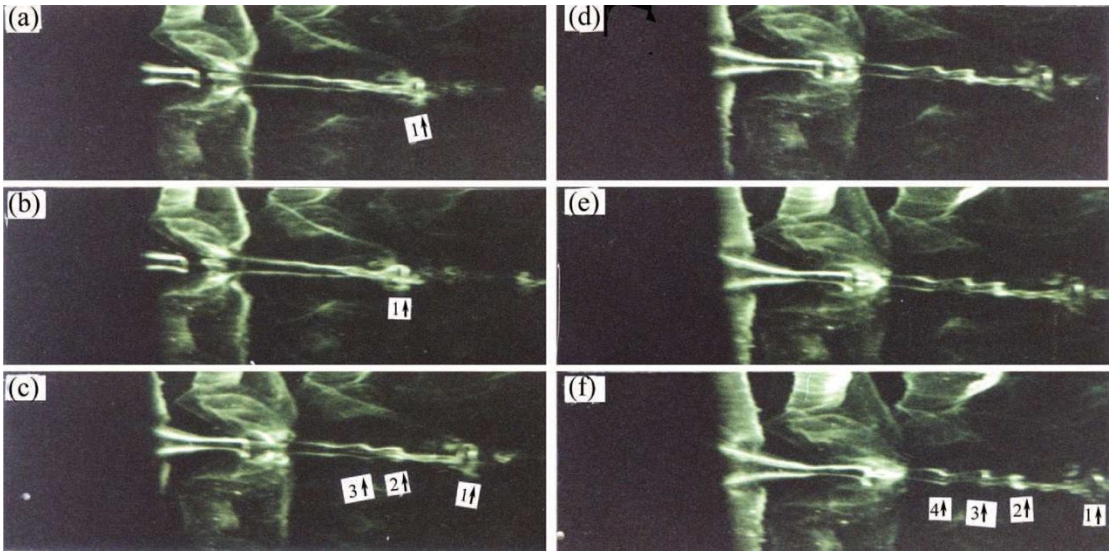

Figure 4-5 Evolution of ring-like vortices by experiment

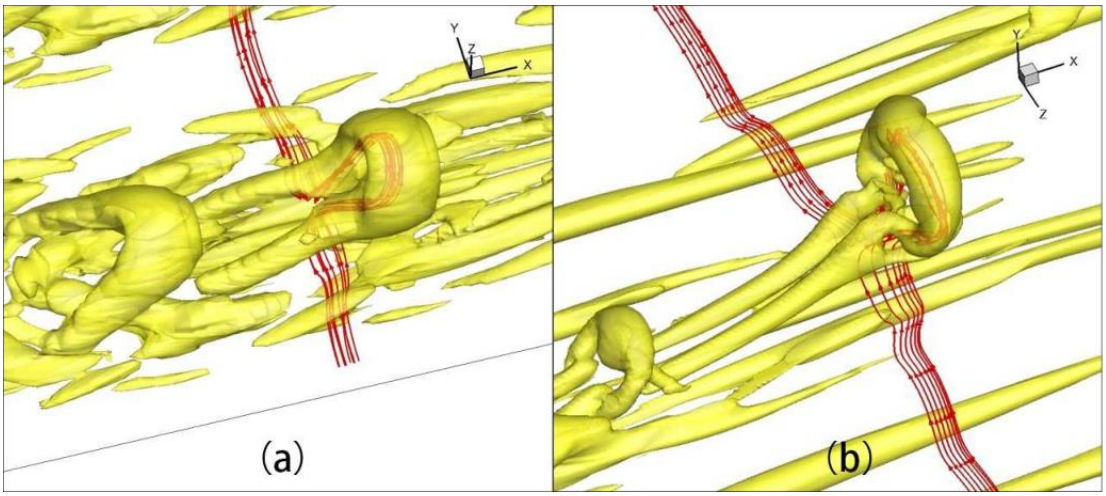

Figure 4-6 Comparison of our DNS results with Rist's DNS data

4.4.3 Comparison with Rist's DNS data

Figure 4-6 shows a comparison between our DNS results with Rist's DNS data [29] provided as his personal kindness. The comparison shows both DNS results can capture the typical vortical structures during transition.

All above verifications and validations show that the DNS results are reliable and accurate.

4.5 DNS Visualization Method

A new visualization method named "Ω criterion" proposed by Liu [60] is used in this thesis to identify the vortices. The "Ω" is defined as the proportion of vorticity and deformation in fluid element motion:

$$\nabla \mathrm{V} = \frac{1}{2}(\nabla V + \nabla V^T) + \frac{1}{2}(\nabla V - \nabla V^T) = S + W \qquad (4.22)$$

Where S is the symmetric while W is the anti-symmetric part of the velocity gradient tensor. S represents deformation and W is related to the whole vorticity.

The square of Frobenius norms of S and W are $\mathrm{a} = \mathrm{trace}(SS^{\mathrm{T}}), \mathrm{b} = \mathrm{trace}(WW^{\mathrm{T}})$, then:

$$\Omega = \frac{\mathrm{b} + \varepsilon}{(a + \varepsilon) + (b + \varepsilon)} \qquad (4.23)$$

$\Omega = 0.52$ is set as the threshold to identify the region where rotation plays a dominant role rather than deformation as a vortex.

Compared with traditional Q or λ_2 criteria, Ω criteria doesn't need to tune the threshold and have clear physical meaning. In addition, it successes to capture both strong and weak vortices simultaneously while both Q and λ_2 criteria fails. When $\Omega = 1.0$, the flow has pure rotation and has no deformation which means the fluid is stiff like solid, but vortex itself is also very stiff like solid. Although Ω is a measurement of fluid stiffness, but it

is a good measurement of flow rotation, i.e., vortex. Therefore, Ω criteria is the best visualization method for us to detect and track the generation of vortices.

Chapter 5

INSTABILITY OF TWO-DIMENSIONAL SHEAR FLOW

5.1 Linear Stability Equation

Consider the Non-dimensional Navier-Stokes equations for incompressible flow:

$$\begin{cases} \dfrac{\partial V}{\partial t} + V \cdot \nabla V = -\nabla p + \dfrac{1}{Re}\nabla^2 V \\ \nabla \cdot V = 0 \end{cases} \tag{5.1}$$

where $\mathrm{V} = (\mathrm{u}, \mathrm{v}, \mathrm{w})$ is the velocity vector with u denotes streamwise component, v denotes normal component, and w denotes spanwise component.

Recall the linear stability theory on section 2.3, we have:

$$\mathrm{q}(x, y, z, t) = q_0(y) + q'(x, y, z, t) \tag{5.2}$$

where q can be specified as (u,v,w,p) and $\mathrm{q}_0 = (\mathrm{u}_0, \mathrm{v}_0, \mathrm{w}_\mathrm{o}, \mathrm{p}_0)$ represents the value of base flow. q' denotes the corresponding linear perturbation.

By eliminating the second order perturbation terms, the linearized governing equation for small perturbations can be written as,

$$\begin{cases} \dfrac{\partial V'}{\partial t} + (V_0 \cdot \nabla)V' + (V' \cdot \nabla)V_0 + \nabla p' = \dfrac{1}{Re}\nabla^2 V' \\ \nabla \cdot V' = 0 \end{cases} \tag{5.3}$$

As a first step, a localized 2-D incompressible temporal stability for shear layer is studied. It relates to the distance among two neighboring vortices in the central streamwise plane. Assume the normal mode is

$$\mathrm{V}' = \hat{\mathrm{V}}(y)e^{i(\alpha x + \beta z - \omega t)} + c.c. = \hat{\mathrm{V}}(y)e^{i\alpha\left(x + \frac{\beta}{\alpha}z - ct\right)} + c.c. \tag{5.4}$$

$$\mathrm{p}' = \hat{\mathrm{p}}(y)e^{i(\alpha x + \beta z - \omega t)} + c.c. = \hat{\mathrm{p}}(y)e^{i\alpha\left(x + \frac{\beta}{\alpha}z - ct\right)} + c.c. \tag{5.5}$$

with $\mathrm{c} = \frac{\omega}{\alpha}$. Here $\hat{\mathrm{V}} = (\hat{u}, \hat{v}, \hat{w})$, the wavenumber α and β are given real numbers. The parameter c should be a complex number. Plugging equations (5.4) and (5.5) into equation (5.3) yields:

$$\mathrm{L}\hat{\mathrm{u}} = Re(Du_0)\hat{v} + i\alpha Re\hat{p}$$

$$\mathrm{L}\hat{\mathrm{v}} = Re(D\hat{p})$$

$$\mathrm{L}\hat{\mathrm{w}} = i\beta Re\hat{p}$$

$$\mathrm{i}(\alpha\hat{\mathrm{u}} + \beta\hat{w}) + D\hat{v} = 0 \tag{5.6}$$

where $\mathrm{L} = [\mathrm{D}^2 - (\alpha^2 + \beta^2) - \mathrm{iRe}(\alpha\mathrm{u}_0 - \omega)]$, and $\mathrm{D} = \frac{\mathrm{d}}{\mathrm{dy}}$.

By eliminating$\hat{\mathrm{u}}, \hat{w}, \hat{p}$, we can obtain the Orr-Sommerfeld equation on $\hat{\mathrm{v}}$,

$$\left(-\mathrm{Uk}^2 - \mathrm{U}'' - \frac{\mathrm{k}^4}{\mathrm{i}\alpha\mathrm{Re}}\right)\hat{\mathrm{v}} + \left(U + \frac{2k^2}{i\alpha Re}\right)\hat{v}'' - \frac{1}{i\alpha Re}\hat{v}'''' = c(\hat{v}'' - k^2\hat{v}) \tag{5.7}$$

where $\mathrm{U} = \mathrm{u}_0$ and $\mathrm{k}^2 = \alpha^2 + \beta^2$.

With boundary conditions

$$\hat{\mathrm{v}}(\pm 1) = \hat{v}'(\pm 1) = 0,$$

Equation (5.7) is an eigenvalue problem about $\hat{v}$ with eigenvalue c. The eigenvalue c determines the property of stability of the equation. Let $c = c_r + ic_i$, if $c_i > 0$, then the disturbance will continuously grow and the flow would be instable. While if c_r is greater, the disturbance will grow faster and the flow would be more unstable. But if $c_i < 0$, the flow would be stable.

Orr-Sommerfeld equation is named after William McFadden Orr and Arnold Sommerfled, who derived is at the beginning of the 20th century. It describes the perturbation of two-dimensional parallel flow, and is widely used in Boundary-layer linear stability theory.

5.2 Chebyshev Discretization of the Orr-Sommerfeld Equation

In this section, a spectral collocation method based on Chebyshev polynomials is applied to the Orr-Sommerfeld equation. This method has advantages to compute the stability characteristics of shear flows as we discussed in Chapter 3.

Recall Equation (5.7), the eigenfunction $\hat{v}$ could be approximated by Chebyshev expansion,

$$\hat{\mathrm{v}}(y) = \sum_{n=0}^{\infty} a_n T_n(y) \approx \sum_{n=0}^{N} a_n T_n(y) \tag{5.8}$$

The derivatives of the eigenfunctions are obtained by differentiating the expansion above. For example, the approximation of the second derivative is,

$$D^2\hat{v}(y) = \sum_{n=0}^{N} a_n T_n''(y) \tag{5.9}$$

And similarly, for the fourth derivative.

Upon substitution into the Orr-Sommerfeld equation we get

$$\sum_{n=0}^{N}\left[\left(-Uk^2 - U'' - \frac{k^4}{i\alpha Re}\right)T_n + \left(U + \frac{2k^2}{i\alpha Re}\right)T_n'' - \frac{1}{i\alpha Re}T_n''''\right]a_n = c\sum_{n=0}^{N} a_n(T_n'' - k^2T_n) \tag{5.10}$$

Chebyshev collocation method is then used, require this equation to be satisfied at the Gauss point (Chebyshev nodes):

$$\mathrm{y_j} = \cos\left(\frac{2j+1}{2N}\pi\right), \qquad j = 0,1,\cdots,N-1 \tag{5.11}$$

The recurrence relations in Chapter 3 () are used to evaluate the derivatives of the Chebyshev polynomials.

The discretized boundary conditions read

$$\sum_{n=0}^{N} a_n T_n(1) = 0 \qquad\qquad \sum_{n=0}^{N} a_n T_n(-1) = 0$$

$$\sum_{n=0}^{N} a_n T_n'(1) = 0 \qquad \sum_{n=0}^{N} a_n T_n'(-1) = 0 \tag{5.12}$$

Applying equation (5.10) on the collocation points grid with boundary conditions above, a matrix form of generalized eigenvalue problem is given by the form

$$\boldsymbol{Aa} = c\boldsymbol{Ba} \tag{5.13}$$

With the right-hand side

$$c\boldsymbol{Ba} =$$

$$c\begin{pmatrix} T_0(1) & T_1(1) & \cdots \\ T_0'(1) & T_1'(1) & \cdots \\ T_0''(y_1) - k^2 T_0(y_1) & T_1''(y_1) - k^2 T_1(y_1) & \cdots \\ \vdots & \vdots & \vdots \\ T_0''(y_N) - k^2 T_0(y_M) & T_1''(y_N) - k^2 T_1(y_M) & \cdots \\ T_0'(-1) & T_1'(-1) & \cdots \\ T_0(-1) & T_1(-1) & \cdots \end{pmatrix} \begin{pmatrix} a_0 \\ a_1 \\ a_2 \\ \vdots \\ a_{N-3} \\ a_{N-2} \\ a_{N-1} \end{pmatrix}$$

and similar for the left-hand side $\boldsymbol{Aa}$. We have chosen to use the first, second, last and next-to-last row of $\boldsymbol{B}$ to implement the four boundary conditions. The same rows in the matrix $\boldsymbol{A}$ can be chosen as a complex multiple of the corresponding rows in $\boldsymbol{B}$. By carefully selecting this complex multiple, the spurious modes associated with the boundary conditions can be mapped to an arbitrary location in the complex plane.

5.3 Numerical results for typical shear flows

Typical shear flow (Figure 5-):

$$U(y) = \tanh(by),\ y \in [-1,1]$$

Computational conditions:

The number of O-S nodes is $N = 100$, streamwise wave number is $\alpha = 1$ and spanwise wave number is β =0.

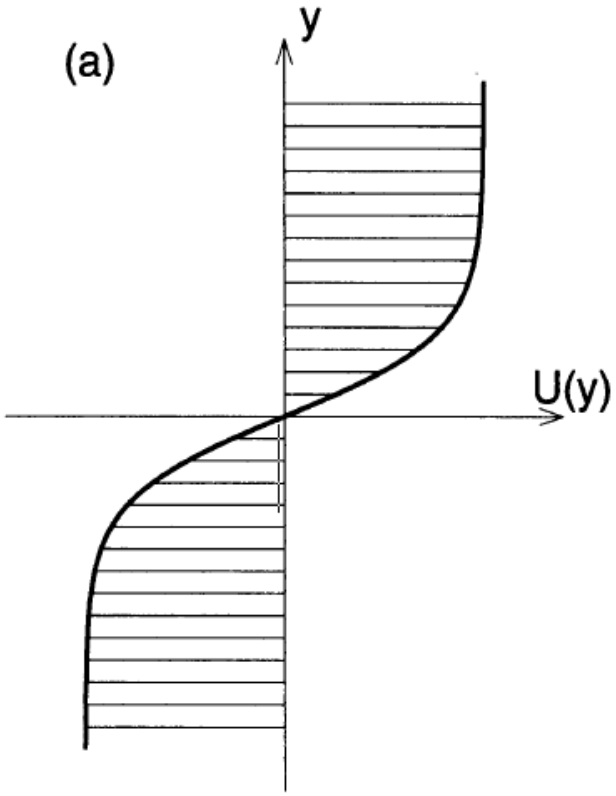

Figure 5-1 Sketch of typical shear flow velocity profile

First, set $b = 2$, Figure 5-2 provides the comparison of spectrums upon base flow $U(y) = \tanh(2y)$ with Reynolds number $Re = 10, 100, 1000$.

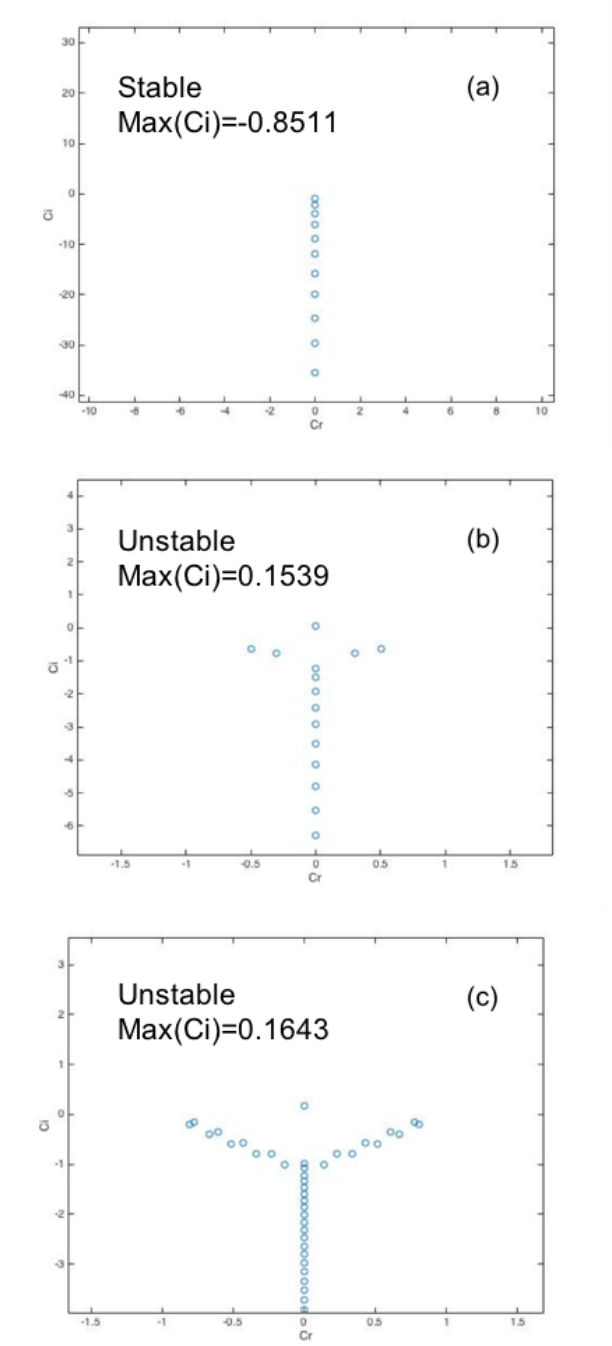

(a) $Re = 10$; (b)$Re = 100$; (c)$Re = 1000$

Figure 5-2 graphs of spectrum on shear flow $U(y) = \tanh(2y)$

Unstable mode (c_i=0.1643) only obtained at $Re = 1000$, the associated eigenfunction $\hat{v}$ is as Figure 5-3:

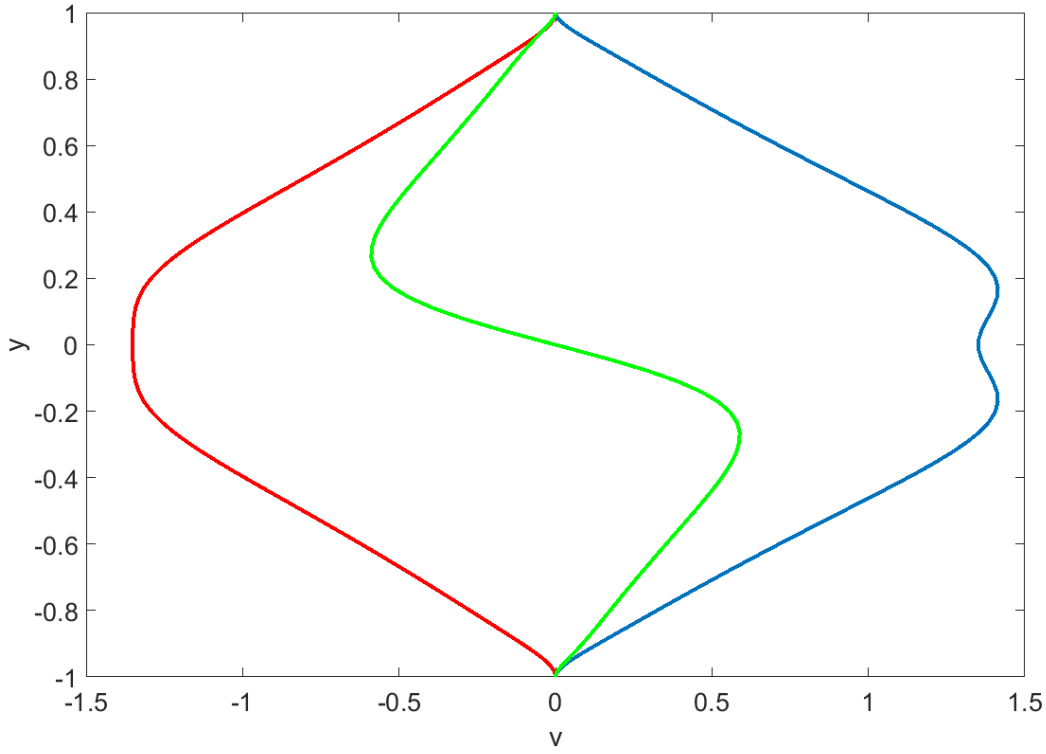

Figure 5-3 Eigenfunction $\hat{v}$ on [-1,1]: red-imag($\hat{v}$); green-real($\hat{v}$); blue-$|\widehat{v}|$

Next, set $\mathrm{b} = 8$, with base flow $\mathrm{U(y)} = \tanh(8\mathrm{y})$, Figure 5-4 provides the comparison of spectrums with Reynolds number $\mathrm{Re} = 10, 100, 1000$.

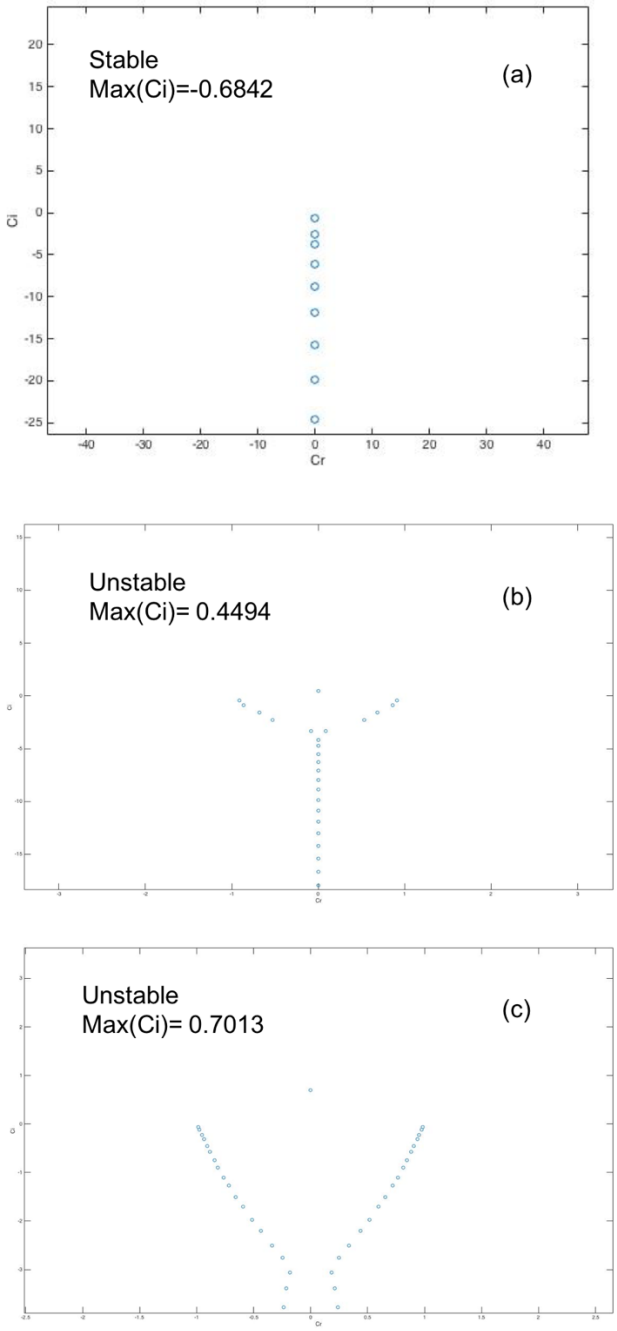

(a) $Re = 10$; (b)$Re = 100$; (c)$Re = 1000$

Figure 5-4 graphs of spectrum on shear flow $U(y) = \tanh(8y)$

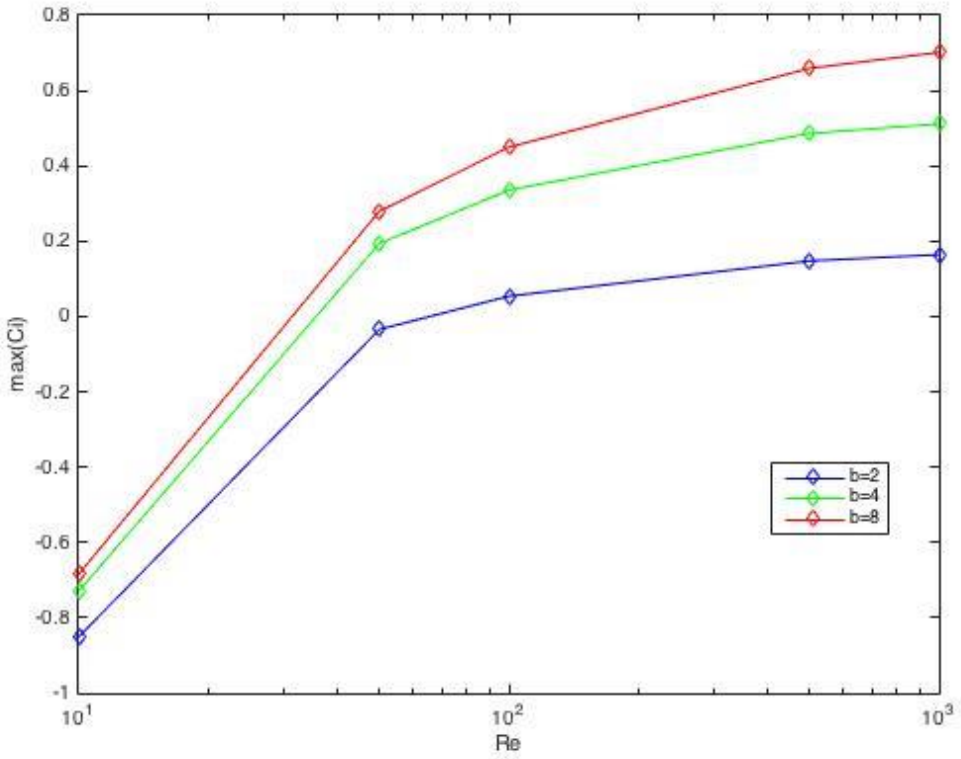

Figure 5-5 Graph of Re and least stable c_i on $b = 2,4,8$.

Consider Figure 5-5, the graph shows that:

(a) For 1-D typical shear flow, it is unstable when Reynolds number is large enough.

(b) The flow is more unstable with the larger Reynolds number and stronger shear stress.

Chapter 6

LINEAR STABILITY EQUATION FOR QUASI-ROTATION FLOW IN CYLINDRICAL COORDINATE

6.1 Derivation of linear perturbation system

The dimensionless NS equations of 2D imcompressible flow can be written in cylindrical coordinates as:

Continuity:

$$\frac{1}{r}\frac{\partial(ru_r)}{\partial r}+\frac{1}{r}\frac{\partial u_\theta}{\partial \theta}=0 \tag{6.1}$$

Radial conservation of momentum:

$$\frac{Du_r}{Dt}-\frac{u_\theta^2}{r}=-\frac{\partial p}{\partial r}+\frac{1}{Re}\left[\nabla^2 u_r-\frac{u_r}{r^2}-\frac{2}{r^2}\frac{\partial u_\theta}{\partial \theta}\right] \tag{6.2}$$

Azimuthal conservation of momentum:

$$\frac{Du_\theta}{Dt}+\frac{u_r u_\theta}{r}=-\frac{\partial p}{\partial \theta}+\frac{1}{Re}\left[\nabla^2 u_\theta-\frac{u_\theta}{r^2}+\frac{2}{r^2}\frac{\partial u_r}{\partial \theta}\right] \tag{6.3}$$

Here,

$$\frac{D}{Dt}\equiv\frac{\partial}{\partial t}+u_r\frac{\partial}{\partial r}+\frac{u_\theta}{r}\frac{\partial}{\partial \theta} \tag{6.4}$$

and

$$\nabla^2\equiv\frac{\partial^2}{\partial r^2}+\frac{1}{r}\frac{\partial}{\partial r}+\frac{1}{r^2}\frac{\partial^2}{\partial \theta^2} \tag{6.5}$$

with u_r, u_θ representing the radial, azimuthal velocity components, p is the pressure, Re is the Reynolds number.

Given the class of steady-state solutions to this system of equations where $u_r = U_0, u_\theta = V_0$, with $p = P_0$, these velocities and pressure must then be solutions to:

$$\frac{1}{r}\frac{\partial(rU_0)}{r}+\frac{1}{r}\frac{\partial V_0}{\partial \theta}=0 \tag{6.6}$$

$$\frac{DU_0}{Dt} - \frac{V_0^2}{r} = -\frac{\partial P_0}{\partial r} + \frac{1}{Re}\left[\nabla^2 U_0 - \frac{U_0}{r^2} - \frac{2}{r^2}\frac{\partial V_0}{\partial \theta}\right] \tag{6.7}$$

$$\frac{DU_0}{Dt} + \frac{U_0 V_0}{r} = -\frac{\partial P_0}{\partial \theta} + \frac{1}{Re}\left[\nabla^2 V_0 - \frac{V_0}{r^2} + \frac{2}{r^2}\frac{\partial U_0}{\partial \theta}\right] \tag{6.8}$$

while satisfying appropriate boundary conditions.

Suppose that the steady-state solution (U_0, V_0, P_0) is subjected to a set of small fluctuations, where

$$u_r = U_0 + u'(r, \theta, t) \tag{6.9}$$

$$u_\theta = V_0 + v'(r, \theta, t) \tag{6.10}$$

$$p = P_0 + p'(r, \theta, t) \tag{6.11}$$

Those fluctuation variables, incorporated with their steady-state components are solutions to the governing equation. According to equations (6.6) -(6.8), the original steady-state part can be removed, leaving:

$$\frac{1}{r}\frac{\partial (ru')}{r} + \frac{1}{r}\frac{\partial v'}{\partial \theta} = 0 \tag{6.12}$$

$$\begin{aligned}\frac{Du'}{Dt} + u'\frac{\partial U_0}{\partial r} - 2\frac{v' V_0}{r} + \frac{\partial u'^2}{\partial r} + \frac{1}{r}\frac{\partial u' v'}{\partial \theta} + \frac{u'^2 - v'^2}{r} \\ = -\frac{\partial p'}{\partial r} + \frac{1}{Re}\left[\nabla^2 u' - \frac{u'}{r^2} - \frac{2}{r^2}\frac{\partial v'}{\partial \theta}\right]\end{aligned} \tag{6.13}$$

$$\begin{aligned}\frac{Dv'}{Dt} + u'\frac{\partial V_0}{\partial r} + \frac{v' U_0 + u' V_0}{r} + \frac{\partial u' v'}{\partial r} + \frac{1}{r}\frac{\partial v'^2}{\partial \theta} + 2\frac{u' v'}{r} \\ = -\frac{1}{r}\frac{\partial p'}{\partial \theta} + \frac{1}{Re}\left[\nabla^2 v' - \frac{v'}{r^2} + \frac{2}{r^2}\frac{\partial u'}{\partial \theta}\right]\end{aligned} \tag{6.14}$$

where

$$\frac{D}{Dt} \equiv \frac{\partial}{\partial t} + U_0 \frac{\partial}{\partial r} + \frac{V_0}{r} \frac{\partial}{\partial \theta} \tag{6.15}$$

The linear stability equations for rotational flow evolve from these fluctuation equations by assuming that quadratic fluctuation terms are negligibly small. Furthermore, we would like to work these equations on cylindrical base flow, hence the general base flow for a vortex in 2D coordinates can be approximated by

$$U_0 \approx 0, V_0 = V_0(r) \tag{6.16}$$

Therefore, the dimensionless, linearized perturbation equations in 2D cylindrical coordinates can be written as:

Continuity:

$$r \frac{\partial u'}{\partial r} + u' + \frac{\partial v'}{\partial \theta} = 0 \tag{6.17}$$

r-Momentum:

$$\frac{\partial u'}{\partial t} + \frac{V_0}{r} \frac{\partial u'}{\partial \theta} - 2 \frac{v' V_0}{r} + \frac{\partial u'^2}{\partial r} = -\frac{\partial p'}{\partial r} + \frac{1}{Re} \left[\nabla^2 u' - \frac{u'}{r^2} - \frac{2}{r^2} \frac{\partial v'}{\partial \theta} \right] \tag{6.18}$$

θ-Momentum:

$$\frac{\partial v'}{\partial t} + u' \frac{\partial V_0}{\partial r} + \frac{V_0}{r} \frac{\partial v'}{\partial \theta} + \frac{u' V_0}{r} + = -\frac{1}{r} \frac{\partial p'}{\partial \theta} + \frac{1}{Re} \left[\nabla^2 v' - \frac{v'}{r^2} + \frac{2}{r^2} \frac{\partial u'}{\partial \theta} \right] \tag{6.19}$$

and

$$\nabla^2 \equiv \frac{\partial^2}{\partial r^2} + \frac{1}{r} \frac{\partial}{\partial r} + \frac{1}{r^2} \frac{\partial^2}{\partial \theta^2} \tag{6.20}$$

6.2 Eigenvalue function

To solve the equations system (6.17) – (6.20), we first subject that system to a normal mode representation of the disturbance field, where

$$\{u', v', p'\} = \{\hat{u}(r), \hat{v}(r), \hat{p}(r)\}e^{i(\alpha\theta - \omega t)} \tag{6.21}$$

Here, u, v and p are amplitude functions which are dependent on the radial coordinate only. For the temporal solution α is the given real and constant wavenumbers in the tangential direction. The angular frequency, ω, is complex and must be computed. The disturbances will grow if the imaginary part of the frequency,ω_i, is positive, and if it is negative the disturbances decay with time. Substituting (6.21) into the governing equation (6.17) – (6.19), we obtain:

Continuity:

$$\hat{u} + rD\hat{u} + i\alpha\hat{v} = 0 \tag{6.22}$$

r-Momentum:

$$(-i\omega)\hat{u} + \frac{i\alpha V_0}{r}\hat{u} - \frac{2V_0}{r}\hat{v} = -D\hat{p} + \frac{1}{Re}\left[\frac{1}{r}D\hat{u} + D^2\hat{u} - \frac{\alpha^2}{r^2}\,\hat{u} - \frac{2i\alpha}{r^2}\,\hat{v} - \frac{\hat{u}}{r^2}\right] \tag{6.23}$$

θ-Momentum:

$$(-i\omega)\hat{v} + DV_0\hat{u} + \frac{i\alpha V_0}{r}\hat{v} + \frac{V_0}{r}\hat{u} = -\frac{i\alpha}{r}\hat{p} + \frac{1}{Re}\left[\frac{1}{r}D\hat{v} + D^2\hat{v} - \frac{\alpha^2}{r^2}\hat{v} + \frac{2i\alpha}{r^2}\hat{u} - \frac{\hat{v}}{r^2}\right] \tag{6.24}$$

where $D = \frac{\partial}{\partial r}$.

Equations (6.22) – (6.24) represent the most general form for this normal model solution to the vortex stability equations for the 2D quasi-cylindrical approximation.

According to the three linear equations system with three variables, it is possible to eliminate two variables $\hat{v}, \hat{p}$ and get a fourth-order ordinary differential equation with respect to $\hat{u}$.

From equation (6.24), the pressure $\hat{p}$ can be expressed in terms of $\hat{u}$ and $\hat{v}$ as follows:

$$\left(\frac{i\alpha}{r}\right)\hat{p} = -\left[(-ic)\hat{v} + DV_0\hat{u} + \frac{i\alpha V_0}{r}\hat{v} + \frac{V_0}{r}\hat{u}\right] + \frac{1}{Re}\left[\frac{1}{r}D\hat{v} + D^2\hat{v} - \frac{\alpha^2}{r^2}\hat{v} + \frac{2i\alpha}{r^2}\hat{u} - \frac{\hat{v}}{r^2}\right] \quad (6.25)$$

$$\hat{p} = \frac{cr}{\alpha}\hat{v} + \frac{ir}{\alpha}DV_0 \cdot \hat{u} - V_0\hat{v} + \frac{i}{\alpha}V_0\hat{u} - \frac{1}{\alpha Re}\left(iD\hat{v} + irD^2\hat{v} - \frac{i\alpha^2}{r}\hat{v} - \frac{2\alpha}{r}\hat{u} - \frac{i}{r}\hat{v}\right) \quad (6.26)$$

Take the derivatives of p, we can get the expression of Dp:

$$Dp = \frac{\partial p}{\partial r} = \frac{c}{\alpha}(v + rDv) + \frac{i}{\alpha}DV_0 \cdot u + \frac{ir}{\alpha}(D^2V_0 \cdot u + DV_0 \cdot Du) - DV_0 \cdot v - V_0Dv$$

$$+ \frac{i}{\alpha}(DV_0 \cdot u + V_0 \cdot Du)$$

$$-\frac{i}{\alpha Re}\left[2D^2v + rD^3v - \alpha^2\left(-\frac{1}{r^2}v + \frac{Dv}{r}\right) - \left(-\frac{1}{r^2}v + \frac{Dv}{r}\right)\right] + \frac{2}{Re}\left(-\frac{1}{r^2}u + \frac{Du}{r}\right) \quad (6.27)$$

Rearrange the equation, get:

$$Dp = \left[\left(\frac{c}{\alpha} - DV_0\right) + \left(-\frac{i}{\alpha Re}\right)\left(\frac{\alpha^2 + 1}{r^2}\right)\right]v + \left[\left(\frac{cr}{\alpha} - V_0\right) + \left(\frac{i}{\alpha Re}\right)\left(\frac{\alpha^2 + 1}{r}\right)\right]Dv$$

$$+\left(-\frac{2i}{\alpha Re}\right)D^2v \quad + \left(-\frac{ir}{\alpha Re}\right)D^3v + \left[\frac{2}{Re}\left(-\frac{1}{r^2}\right) + \frac{i}{\alpha}(2DV_0 + rD^2V_0)\right]u + \left[\frac{2}{rRe} + \frac{i}{\alpha(r \cdot DV_0 + V_0)}\right]Du \quad (6.28)$$

Combine Equation (6.23) and (6.28), get an equation LS=0. Terms with respect to each velocity component on LS is as following individually:

$$
\begin{aligned}
u: &\quad -ic + \frac{i\alpha V_0}{r} + \frac{1}{Re}\left(\frac{\alpha^2+1}{r^2}\right) + \frac{2}{Re}\left(-\frac{1}{r^2}\right) + \frac{i}{\alpha}(2DV_0 + rD^2V_0) \\
Du: &\quad +\frac{1}{rRe} + \frac{i}{\alpha}(r\cdot DV_0 + V_0) \\
D^2u: &\quad -\frac{1}{Re} \\
v: &\quad -\frac{2V_0}{r} + \frac{1}{Re}\left(\frac{2i\alpha}{r^2}\right) + \left(\frac{c}{\alpha} - DV_0\right) + \left(-\frac{i}{\alpha Re}\right)\left(\frac{\alpha^2+1}{r^2}\right) \\
Dv: &\quad +\frac{cr}{\alpha} - V_0 + \frac{i}{\alpha Re}\left(\frac{\alpha^2+1}{r}\right) \\
D^2v: &\quad -\frac{2i}{\alpha Re} \\
D^3v: &\quad -\frac{i}{\alpha r Re}
\end{aligned}
\tag{6.29}
$$

Consider Equation (6.22), all v-velocity components can be replaced by u-velocity components since they have the relations as below:

$$
\begin{aligned}
v &= \frac{i}{\alpha}(u + r\cdot Du) \\
Dv &= \frac{i}{\alpha}(2Du + r\cdot D^2u) \\
D^2v &= \frac{i}{\alpha}(3D^2u + r\cdot D^3u) \\
D^3v &= \frac{i}{\alpha}(4D^3u + r\cdot D^4u)
\end{aligned}
\tag{6.30}
$$

Consider Equation (6.29) and (6.30), a new equation $LS^* = 0$ can be obtained with only u-velocity components on LS^*:

$$
\begin{aligned}
u\text{:}\quad & \frac{1}{r^2 Re}\left(\alpha - \frac{1}{\alpha}\right)^2 + i\left[\frac{V_0}{r}\left(\alpha - \frac{2}{\alpha}\right) + \frac{1}{\alpha}(DV_0 + r \cdot D^2 V_0)\right] + ic\left(\frac{1}{\alpha} - \alpha\right) \\
Du\text{:}\quad & -\frac{1}{rRe}\left(2 + \frac{1}{\alpha^2}\right) - i\left(\frac{3V_0}{\alpha}\right) + ic\left(\frac{3r}{\alpha}\right) \\
D^2u\text{:}\quad & \frac{1}{Re}\left(\frac{5}{\alpha^2} - 2\right) + i\left(-\frac{V_0 r}{\alpha}\right) + ic\left(\frac{r^2}{\alpha}\right) \\
D^3u\text{:}\quad & \frac{1}{Re}\left(\frac{6r}{\alpha^2}\right) \\
D^4u\text{:}\quad & \frac{1}{Re}\left(\frac{r^2}{\alpha^2}\right)
\end{aligned}
\tag{6.31}
$$

Multiply LS^* by $\alpha^2 Re$, we get:

$$
\begin{aligned}
u\text{:}\quad & \frac{1}{r^2}(\alpha^2 - 1)^2 + iRe\left[\frac{\alpha V_0}{r}(\alpha^2 - 2) + \alpha(DV_0 + r \cdot D^2 V_0)\right] + icRe(1 - \alpha^2) \\
Du\text{:}\quad & -\frac{1}{r}(2\alpha^2 + 1) - iRe(3V_0\alpha) + icRe(3r) \\
D^2u\text{:}\quad & (5 - 2\alpha^2) - iRe(2V_0 r) + icRer^2 \\
D^3u\text{:}\quad & 6r \\
D^4u\text{:}\quad & r^2
\end{aligned}
\tag{6.32}
$$

Rearrange equation (6.32), we obtain an ordinary differential equation with respect to the u-velocity components, it is also an eigenvalue function describing the linear modes of disturbance to a quasi-rotation flow. Similar with Orr-Sommerfeld equation, this equation determines what the conditions for flow stability are:

$$D^4u \cdot r^4 + D^3u \cdot 6r^3 + D^2u \cdot r^2[(5 - 2\alpha^2) - i\alpha ReV_0 r]$$
$$+Du \cdot r[-(2\alpha^2 + 1) - 3i\alpha ReV_0 r] + u\{(\alpha^2 - 1)^2 + i\alpha Rer[V_0(\alpha^2 - 2) + rDV_0 + r^2D^2V_0]\}$$
$$= -c \cdot iRer[D^2u \cdot r^3 + Du \cdot 3r^2 + u \cdot (1 - \alpha^2)r] \qquad (6.26)$$

with the boundary conditions:

$$u(0) = 0, \qquad u(1) = 0$$
$$u'(0) = 0, \qquad u'(1) = 0 \qquad (6.27)$$

c represents the angular frequency. Let $\mathrm{c} = \mathrm{c_r} + c_i$. The imaginary part, c_i, determines the stability of the perturbation. It is stable if c_i is negative and unstable if c_i is positive.

6.3 Shifted Chebyshev polynomials and discretization

Since equation (6.25) is based on cylindrical coordinate on a finite domain in radius, the domain is always being normalized to $\mathrm{r} \in [0,1]$, Chebyshev polynomials are no longer available for this problem. A common way to solve it is Shifted Chebyshev polynomials by a linear change-of-coordinate.

6.3.1 Shifted Chebyshev polynomials with linear argument

Define n orthogonal polynomials satisfying

$$T_n^*(r) = T_n(2r-1) = cos(n\, cos^{-1}(2r-1)), \qquad \mathrm{n} = 0,1,2,\cdots \tag{6.28}$$

for $r \in [0,1]$ with n is the order of polynomials.

Therefore, $|T_n^*(r)|$ also bounded by 1.

By setting $2r-1 = cos\theta$, we have:

$$T_n^* = cosn\theta \tag{6.29}$$

Shifted Chebyshev polynomials keep most characters of Chebyshev polynomials. First few polynomials of shifted Chebyshev of linear argument are:

$$T_0^* = 1$$

$$T_1^* = 2r-1$$

$$T_2^* = 8r^2 - 8r + 1$$

$$T_3^* = 32r^3 - 48r^2 + 18r - 1$$

$$T_4^* = 128r^4 - 256r^3 + 160r^2 - 32r + 1 \tag{6.30}$$

Similar with Chebyshev polynomials, shifted Chebyshev polynomials also have the recurrence relationship for polynomials:

$$T_{n+1}^*(r) = (4r-2)T_n^*(r) - T_{n-1}^*(r) \tag{6.31}$$

A recurrence relation on the derivative also can easily be obtained. First, the differentiation of $\mathrm{T}_n^*(r)$ gives:

$$T_n^{*\prime(r)} = \frac{d}{d\theta}(cosn\theta)\frac{d\theta}{dr}$$

$$= \frac{d}{d\theta}(cosn\theta)\frac{1}{\frac{dr}{d\theta}}$$

$$= -nsin(n\theta)\frac{1}{\frac{(-1)sin\theta}{2}}$$

$$= 2n\frac{sin(n\theta)}{\sin\theta}. \qquad (6.32)$$

Then, by the application of trigonometrical formulas, we get the relation:

$$\frac{T_{n+1}^{*\prime}(r)}{n+1} - \frac{T_{n-1}^{*\prime}(r)}{n-1} = 4T_n^*(r) \qquad (6.33)$$

with $T_0^{*\prime}(r) = 0$ and $T_1^{*\prime}(r) = 2$.

6.3.2 Shifted Chebyshev polynomials with quadratic argument

In cylindrical or polar coordinates, the shifted Chebyshev polynomials with linear argument is usual a bad option. The reason is that the Shifted-Chebyshev grid has points clustered near both $r = 0$ and $r = 1$. However, the disk bounded by $r = \rho$ has an area which is only the fraction ρ^2 of the area of the unit disk. Near the origin, points are separated by $O(1/N^2)$. It follows that the high density of points near the origin is giving high resolution of only a tiny, $O(1/N^4)$ in the area portion of the disk.

The Shifted Chebyshev polynomials of quadratic argument is a good alternate of the linear argument. It is defined as:

$$T_n^{**}(r) = T_n(2r^2 - 1) = cos(n\, cos^{-1}(2r^2 - 1)), \qquad \mathrm{n} = 0,1,2,\cdots \tag{6.34}$$

for $r \in [0,1]$ with n is the order of polynomials.

Figure 6-1 shows the points of two different Shifted Chebyshev series on $[0,1]$.

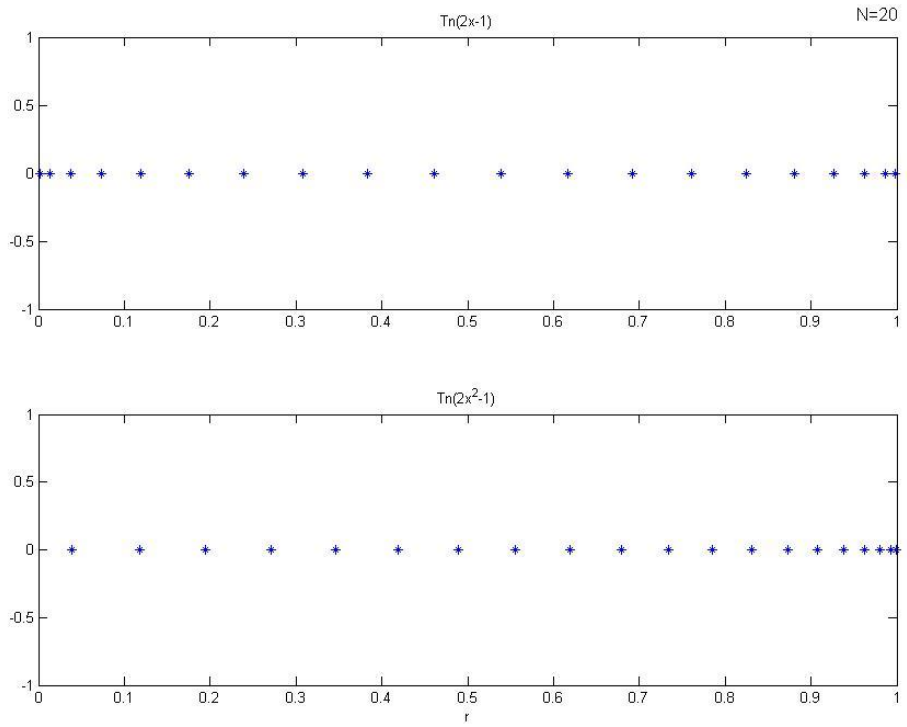

Figure 6-1 Chebyshev nodes distribution of two Shifted-Chebyshev series on [0,1] with N=20.

By setting $2r^2 - 1 = cos\theta$, we have:

$$T_n^{**} = cosn\theta \tag{6.35}$$

First few polynomials of shifted Chebyshev of quadratic argument are:

$$T_0^{**} = 1$$

$$T_1^{**} = 2r^2 - 1$$

$$T_2^{**} = 8r^4 - 8r^2 + 1$$

$$T_3^{**} = 32r^6 - 48r^4 + 24r^2 - 3r - 4 \tag{6.36}$$

The recurrence relationship for Shifted Chebyshev polynomials of quadratic is:

$$T_{n+1}^{**}(r) = (4r^2 - 2)T_n^{**}(r) - T_{n-1}^{**}(r) \tag{6.37}$$

A recurrence relation on the derivative also can easily be obtained. First, the differentiation of $\mathrm{T}_n^*(r)$ gives:

$$T_n^{*\prime(r)} = \frac{d}{d\theta}(cosn\theta)\frac{d\theta}{dr}$$

$$= \frac{d}{d\theta}(cosn\theta)\frac{1}{\frac{dr}{d\theta}}$$

$$= -nsin(n\theta)\frac{1}{\frac{(-1)sin\theta}{4r}}$$

$$= 4nr\frac{sin(n\theta)}{\sin\theta}. \qquad (6.38)$$

Then, by the application of trigonometrical formulas, we get the relation:

$$\frac{T_{n+1}^{**\prime}(r)}{n+1} - \frac{T_{n-1}^{**\prime}(r)}{n-1} = 4rT_n^{**}(r) \qquad (6.39)$$

with $T_0^{*\prime}(r) = 0$ and $T_1^{*\prime}(r) = 4r$.

6.3.3 Equation discretization

Recall equation (6.25), the independent variable of this ordinary differential equation is $u(r)$. In linear stability analysis, the function $u(r)$ could be approximated by

$$u(r) = \sum_{n=0}^{\infty} a_n T_n^*(r) \approx \sum_{n=0}^{N-1} a_n T_n^*(r)\,, \qquad (6.40)$$

or

$$u(r) = \sum_{n=0}^{\infty} a_n T_n^{**}(r) \approx \sum_{n=0}^{N-1} a_n T_n^{**}(r)\,, \qquad (6.41)$$

where N is the number of Chebyshev polynomials used to approximate the velocity profile, T_n^* is Shifted Cheybshev polynomials of linear argument and T_n^{**} is of quadratic argument. a_n are the coefficients.

Equations (6.25) and (6.33) give

$$\sum_{n=0}^{N-1}\{r^4\cdot T_n''''+6r^3\cdot T_n'''+r^2[(5-2\alpha^2)-i\alpha ReV_0 r]\cdot T_n''+r[-(2\alpha^2+1)-3i\alpha ReV_0 r]\cdot T_n'$$
$$+\{(\alpha^2-1)^2+i\alpha Rer[V_0(\alpha^2-2)+rDV_0+r^2D^2V_0]\}\cdot T_n\}a_n$$
$$=c\sum_{n=0}^{N-1}\{iRer[r^3\cdot T_n''+3r^2\cdot T_n'+(1-\alpha^2)r\cdot T_n]\}a_n \qquad (6.42)$$

For convenience, here T_n represents T_n^* or T_n^{**}.

Use Chebyshev nodes in the interval $(0,1)$ to determine r_j:

$$r_j=\frac{1}{2}\left[cos\left(\frac{2j+1}{2M}\pi\right)+1\right],\qquad j=0,1,\dots,M-1 \qquad (6.43)$$

$$r_j=\frac{1}{2}\left[\cos\left(\frac{2j+1}{2M}\pi\right)+1\right]^{\frac{1}{2}},\qquad j=0,1,\dots,M-1 \qquad (6.44)$$

The boundary conditions are $u(0)=u'(0)=0$ and $u(1)=u'(1)=0$:

$$\sum_{n=0}^{N-1}a_nT_n(0)=0,\qquad \sum_{n=0}^{N-1}a_nT_n'(0)=0,$$
$$\sum_{n=0}^{N-1}a_nT_n(1)=0,\qquad \sum_{n=0}^{N-1}a_nT_n'(1)=0. \qquad (6.45)$$

The derivatives have the following recurrence relation for linear argument:

$$\mathrm{T}_n^{(k)}(r_j) = 4nT_{n-1}^{(k-1)}(r_j) + \frac{n}{n-2}T_{n-2}^{(k)}(r_j), \qquad n = 3,4,\cdots \tag{6.46}$$

The first three terms from the first derivative to the forth derivative are:

$$\begin{gathered}
\mathrm{T}_0'(r_j) = 0, \qquad \mathrm{T}_1'(r_j) = 2, \qquad \mathrm{T}_2'(r_j) = 8r - 16, \\
\mathrm{T}_0''(r_j) = 0, \qquad \mathrm{T}_1''(r_j) = 0, \qquad \mathrm{T}_2''(r_j) = 16, \\
\mathrm{T}_0'''(r_j) = 0, \qquad \mathrm{T}_1'''(r_j) = 0, \qquad \mathrm{T}_2'''(r_j) = 0, \\
\mathrm{T}_0''''(r_j) = 0, \qquad \mathrm{T}_1''''(r_j) = 0, \qquad \mathrm{T}_2''''(r_j) = 0.
\end{gathered} \tag{6.47}$$

Apply equation (6.34) on the whole Chebyshev nodes with boundary conditions (6.43), a matrix form of generalized eigenvalue problem is given by the form

$$\boldsymbol{Aa} = \boldsymbol{cBa}. \tag{6.48}$$

Matrix $\boldsymbol{A}$ and $\boldsymbol{B}$ have $(M+4) * N$ dimension. The size of row is $M+4$ not M, the reason is that the Chebyshev Nodes do not conclude two boundary points, four rows of boundary conditions are thus added to Matrix A.

The right hand side $c\boldsymbol{Ba} =$

$$c\begin{pmatrix} T_0(1) & T_1(1) & \cdots \\ T_0'(1) & T_1'(1) & \cdots \\ T_0''(y_1) - k^2T_0(y_1) & T_1''(y_1) - k^2T_1(y_1) & \cdots \\ \vdots & \vdots & \vdots \\ T_0''(y_M) - k^2T_0(y_M) & T_1''(y_M) - k^2T_1(y_M) & \cdots \\ T_0'(0) & T_1'(0) & \cdots \\ T_0(0) & T_1(0) & \cdots \end{pmatrix}\begin{pmatrix} a_0 \\ a_1 \\ a_2 \\ \vdots \\ a_{N-3} \\ a_{N-2} \\ a_{N-1} \end{pmatrix} \tag{6.49}$$

The matrix form of this system can be written as

$$\boldsymbol{B}^{g}\boldsymbol{A}\boldsymbol{a} = c\boldsymbol{a}. \tag{6.50}$$

$\boldsymbol{B}^{g}$ represents the generalized inverse matrix of $\boldsymbol{B}$ with $(M+4)*N$, it can be obtained by using least squares. c appears as eigenvalue of matrix $\boldsymbol{B}^{g}\boldsymbol{A}$ with the associated eigenfunction $\hat{u}(r) = \sum_{n=0}^{N-1} a_n T_n(r)$.

Then we have a set of flow modes, denoted as $\{u_n, c_n\}_{n=0}^{N-1}$. Note that if c_n has greatest imaginary part, then associated u_n is most unstable.

For quadratic argument, the derivatives have the following recurrence relation:

$$\mathrm{T}_n^{(k)}(r_j) = 4nrT_{n-1}^{(k-1)}(r_j) + \frac{n}{n-2}T_{n-2}^{(k)}(r_j), \qquad n = 3,4,\cdots \tag{6.51}$$

The first three terms from the first derivative to the forth derivative are:

$$\begin{gathered}
\mathrm{T}_0'(r_j) = 0, \qquad \mathrm{T}_1'(r_j) = 4r, \qquad \mathrm{T}_2'(r_j) = 16r(2r^2-1), \\
\mathrm{T}_0''(r_j) = 0, \qquad \mathrm{T}_1''(r_j) = 4, \qquad \mathrm{T}_2''(r_j) = 96r^2 - 16, \\
\mathrm{T}_0'''(r_j) = 0, \qquad \mathrm{T}_1'''(r_j) = 0, \qquad \mathrm{T}_2'''(r_j) = 192r, \\
\mathrm{T}_0''''(r_j) = 0, \qquad \mathrm{T}_1''''(r_j) = 0, \qquad \mathrm{T}_2''''(r_j) = 192.
\end{gathered} \tag{6.52}$$

Recall equations (6.46) and (6.47), for quadratic case, the dimension of $\boldsymbol{A}$, $\boldsymbol{B}$ and $\boldsymbol{B}^{g}$ is $(M+3)*N$, the reason is that the derivative of $T_n(0)$ is always be zero since every term contains r:

$$T_n'(0) = 0 \ \ for\ all\ n = 0,1,\cdots,N-1.$$

The right hand side $c\boldsymbol{Ba} =$

$$c\begin{pmatrix} T_0(1) & T_1(1) & \cdots \\ T_0'(1) & T_1'(1) & \cdots \\ T_0''(y_1) - k^2T_0(y_1) & T_1''(y_1) - k^2T_1(y_1) & \cdots \\ \vdots & \vdots & \vdots \\ T_0''(y_M) - k^2T_0(y_M) & T_1''(y_M) - k^2T_1(y_M) & \cdots \\ T_0(0) & T_1(0) & \cdots \end{pmatrix}\begin{pmatrix} a_0 \\ a_1 \\ a_2 \\ \vdots \\ a_{N-3} \\ a_{N-2} \\ a_{N-1} \end{pmatrix} \tag{6.53}$$

Chapter 7

DNS OBSERVATIONS AND NUMERICAL RESULTS

7.1 Comparison of two shifted Chebyshev polynomials in a hyperbolic case

To test the convergence property of two shifted Chebyshev polynomials, a hyperbolic function $V_0 = tanh(5r)$ is used as the velocity of base flow to solve the linear system (6.48).

Figure 7-1 shows the velocity profile of the base flow, the first derivative term DV_0 and the second derivative term DDV_0 can be easily obtained by the hyperbolic function. For this base flow, the gradient of velocity is large near $r = 0$ and is almost zero near $r = 1$.

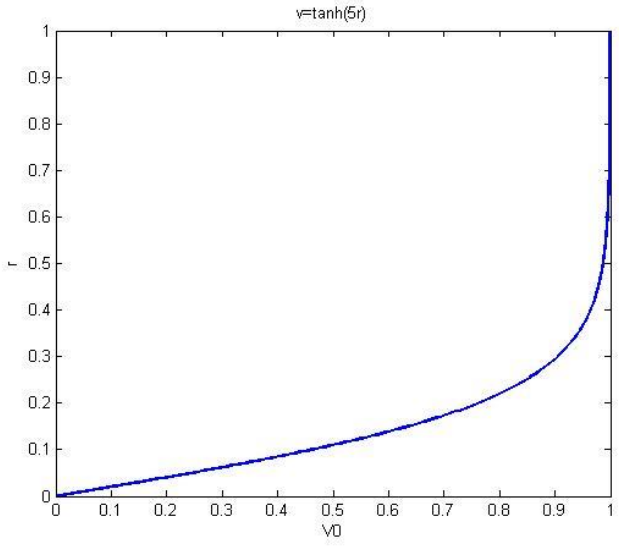

Figure 7-1 Illustration of hyperbolic function $v = tanh(5r)$ on $r \in [0,1]$

Recall Equation (6.41) The problem is solved by using MATLAB, given $Re = 1000$, $\alpha = 1$, and $N = M = 100$. Figure 7-2 gives the results of using Shifted Chebyshev of linear transformation, the distribution of imaginary part of eigenvalues c (i.e. c_i). In Figure 7-2(b), one positive c_i is presented, it represents one unstable mode with $c_i = 0.2004$. The graph of this unstable mode is shown in Figure 7-3. The eigenfunction $v = \sum_0^{N-1} a_n T_n$ is complex, thus Figure 7-3 provides the real part, imaginary part and modulus of it.

The distribution of imaginary eigenvalues c_i and graph of unstable mode ($c_i = 0.2213$) under Shifted Chebyshev polynomials of quadratic transformation are presented in Figure 7-4 and Figure 7-5.

Recall the previous section, the different basis functions present different collocation points. Upon linear Shifted Chebyshev polynomials, points clustered near both $r = 0$ and $r = 1$; while upon quadratic Shifted Chebyshev polynomials, they only clustered near $r = 1$.

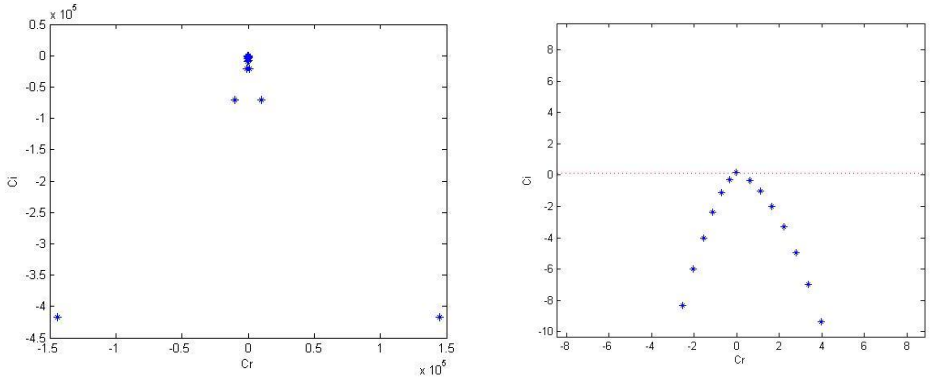

(a) Global view (b) Zoom-in view

Figure 7-2 spectrum distribution of using $\mathrm{T_n}(2r-1)$

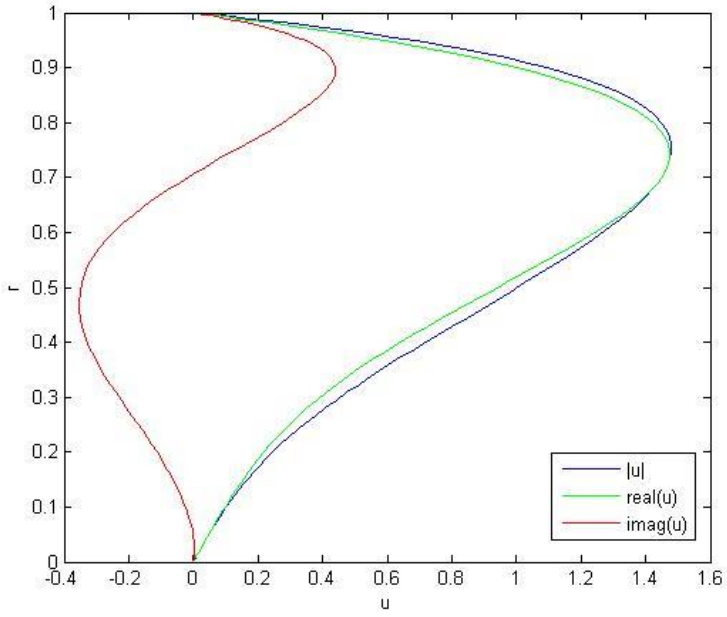

Figure 7-3 Eigenfunction û associated with $c = -0.0102 + 0.2004\mathrm{i}$ on $\mathrm{T_n}(2r-1)$

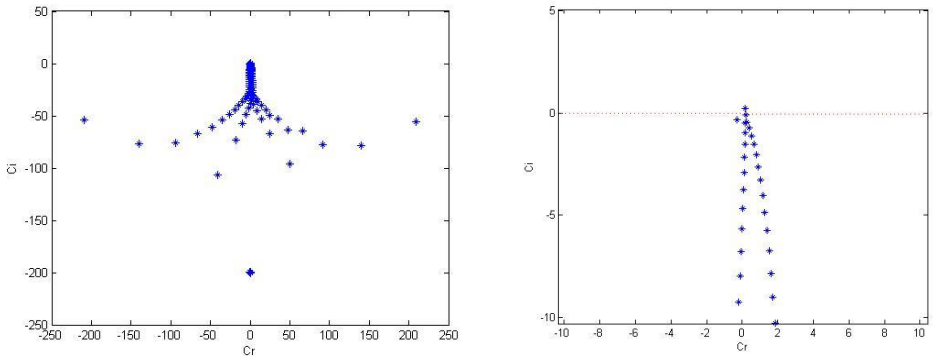

(a) Global view (b) Zoom-in view

Figure 7-4 spectrum distribution of using $\mathrm{T_n}(2r^2-1)$

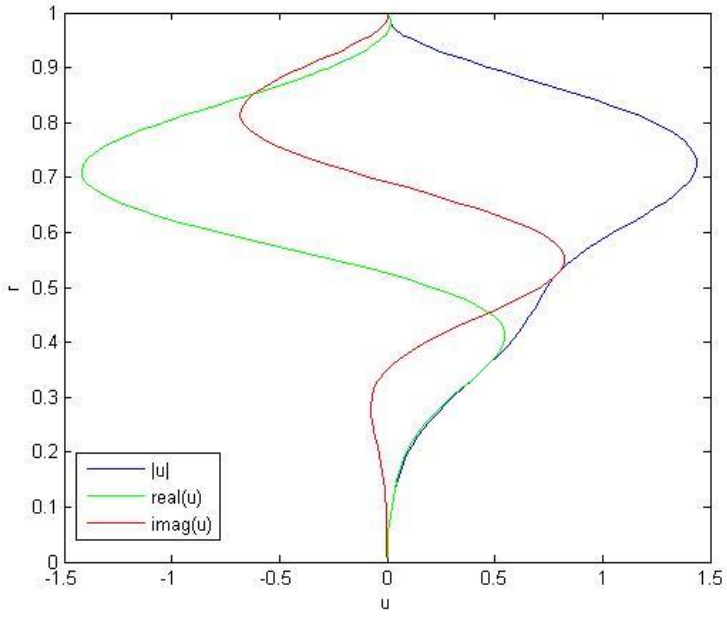

Figure 7-5 Eigenfunction û associated with $\mathrm{c} = \ 0.1709 \ + \ 0.22146\mathrm{i}$ on $\mathrm{T_n}(2r^2-1)$

The Convergence property of the Chebyshev Collocation Method upon two Shifted Chebyshev polynomials is listed in Table 7-1. M is the number of grid points (Chebyshev nodes). In Table 7-1, with M increased gradually, the convergence of the eigenvalues on quadratic Shifted Chebyshev polynomials is observed, while eigenvalues on linear Shifted Chebyshev polynomials are not convergent. The results by using linear transformation are not reliable.

In quadratic case, four-digit accuracy is obtained.

Table 7-1 The Convergence property of c_i on two Shifted Chebyshev Polynomials

M	$T_n(2r-1)$	$T_n(2r^2-1)$
100	0.20044245	0.22127542
120	0.20780676	0.22145990
140	0.21363761	0.22146397
160	0.21835979	0.22145546
180	0.22225536	0.22147179
200	0.22552000	0.22146576
400	0.24190921	0.22145805
800	0.25114780	0.22146244

7.2 DNS leg-like vortices cases

Section 7.1 shows the convergence property of Chebyshev collocation method with different basis functions (linear and quadratic transformation) with base flow as a mathematical hyperbolic function. In this and next section, quasi-rotation flow in our DNS data are carefully discussed in this and next section. Quasi-rotation flow locates on the core of vortex structure, it can be well captured with Ω vortex identification method.

Hairpin vortices are widely recognized as a fundamental coherent structure since their appearance in every significant process during transition. The hairpin vortex usually consists of three parts: (1) Two counter-rotating quasi-streamwise vortices, known as two legs; (2) A ring-like vortex named as the vortex head, where the spanwise vorticity is dominant, sitting on top farther from the wall, (3) Necks connect the head and legs.

In this section, the DNS observation and numerical results of stability based on leg-like vortex are discussed. The other typical vortex, ring-like vortex, is discussed in next section.

7.2.1 DNS observations

Figure 7-6 provides the structure of transition flow at $t = 6.87T$, T is the period. The spanwise tubes and hairpin vortices are captured at $\Omega = 0.5$, the spanwise tubes cannot represent rotation. With stretch and distortion, the tubes become Hairpin vortices gradually. Leg-like vortices are generated within this process.

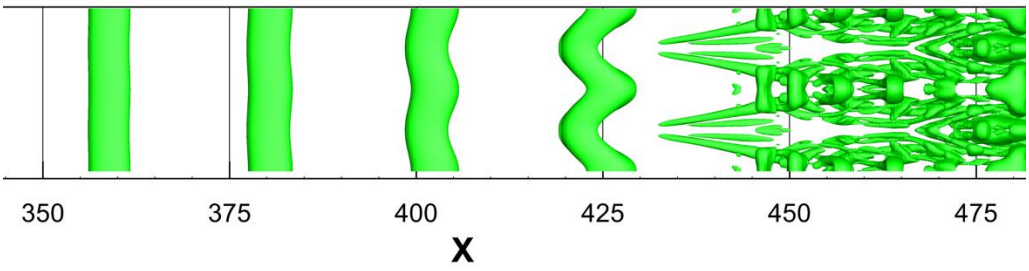

Figure 7-6 X-Z view of the transition flow at $\Omega = 0.5$ on $t = 6.87T$

Figure 7-7 give the distribution of shear on three directions on certain sections of spanwise tubes. Figure 7-8 shows the generation of leg-like vortices with $\Omega = 0.52$, the isosurface describes rotation with the reason $\Omega > 0.5$ based on the Ω vortex identification method.

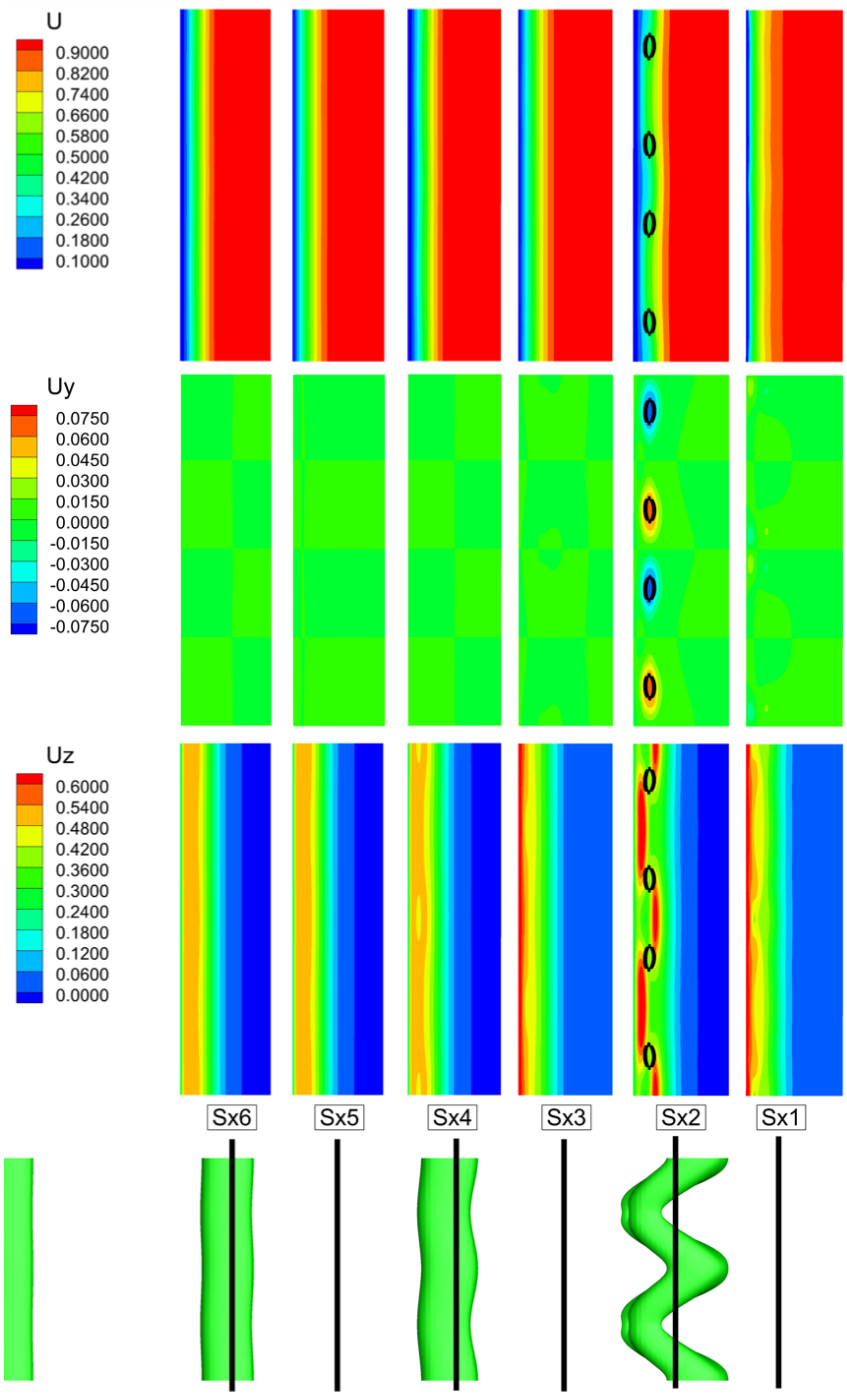

Figure 7-7 distribution of u-velocity and correlated shear stress on certain six slices

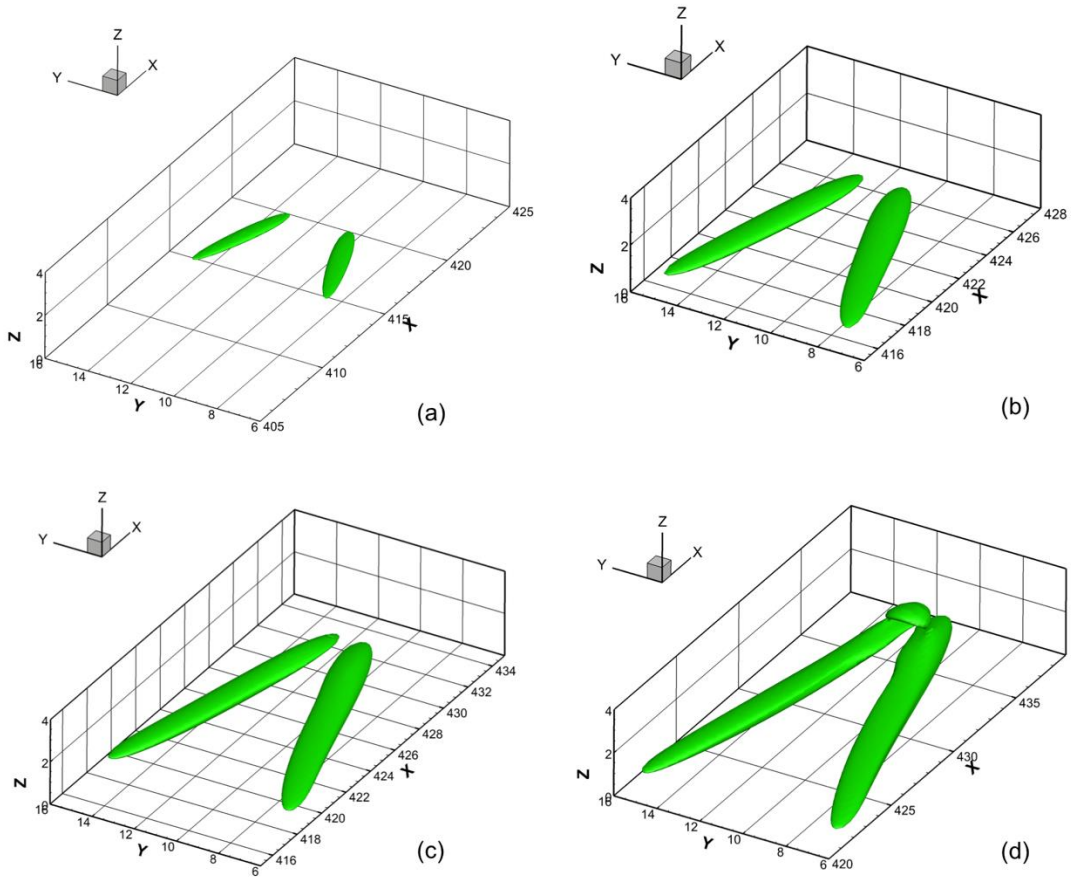

Figure 7-8 Generation of one leg-like vortex at $\Omega = 0.52$ on

(a) t=5.87T; (b) t=6.01T; (c) t=6.16T; (d) t=6.30T

To investigate the quasi-rotation flow with leg-like vortex, a fully developed leg is shown in Figure 7-9. Figure 7-10 depicts three y-section located in $x = 430.6$, 434.7 and 439.8.

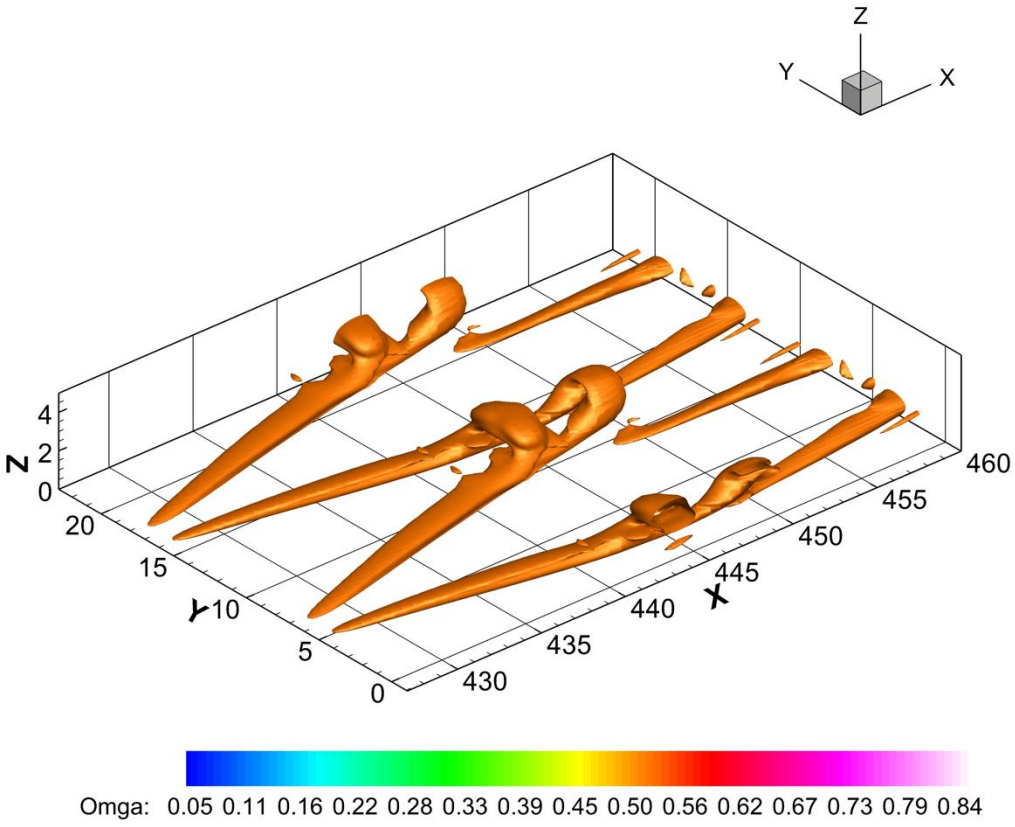

Figure 7-9 Fully developed leg-like vortices ($x = 427$ to 440) at $\Omega = 0.52$ on $t = 6.60T$

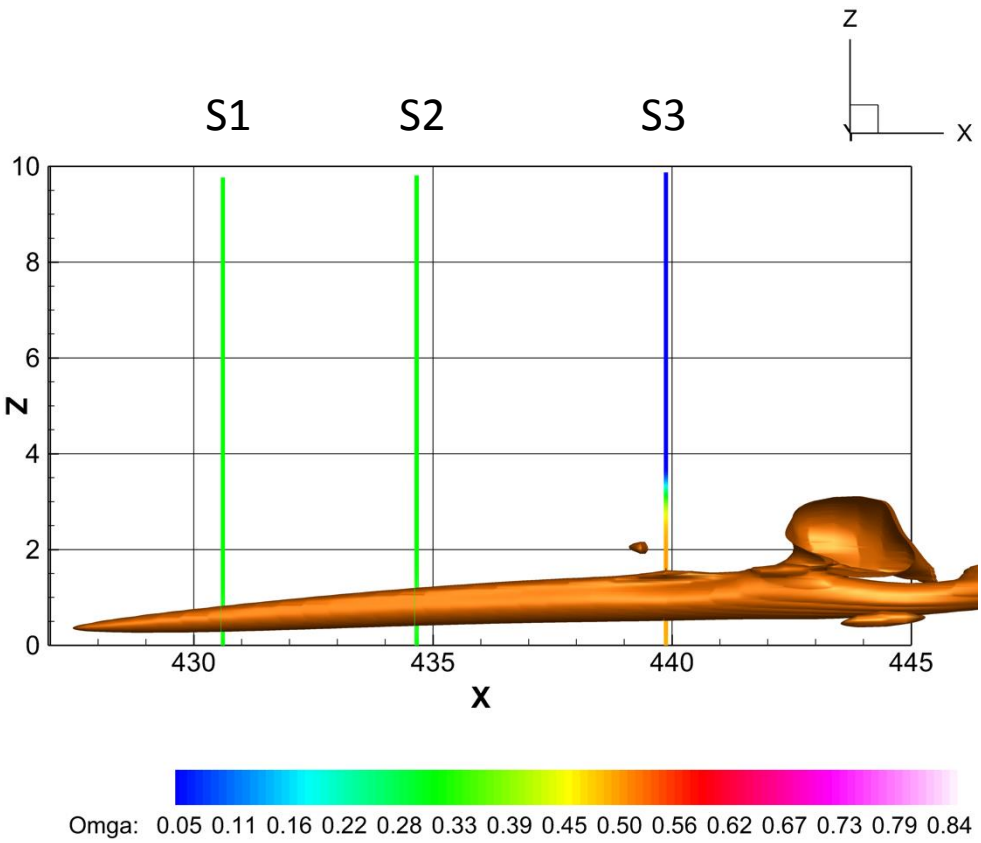

Figure 7-10 x-z view of leg-like vortex with three y-sections

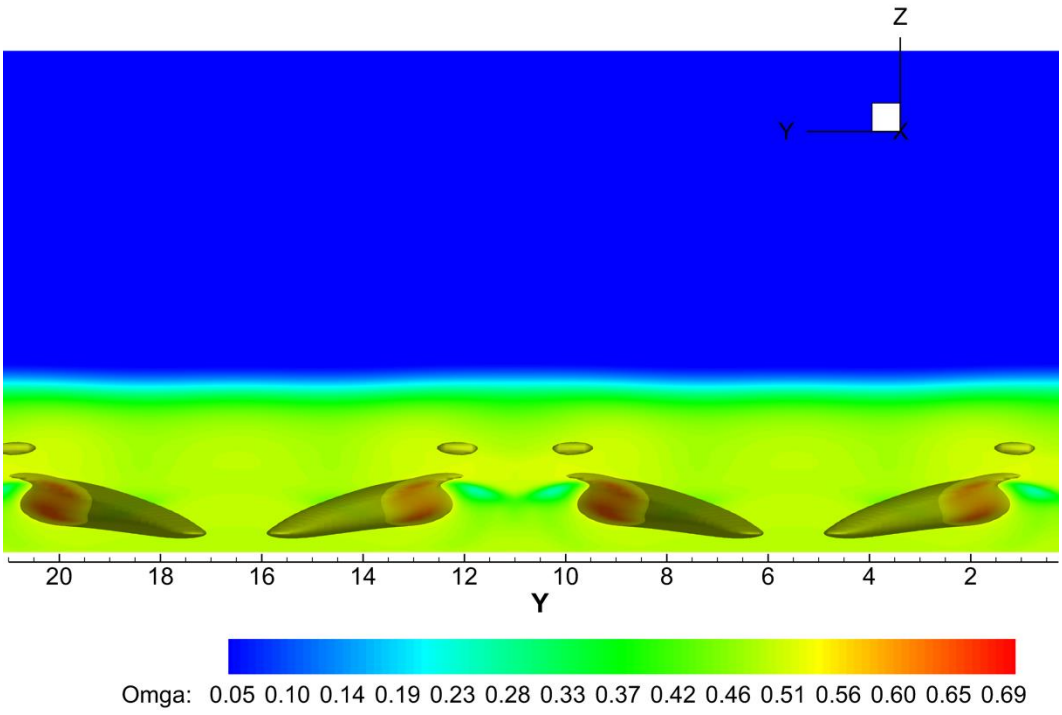

Figure 7-11 y-section slice at $x = 439.8$ with Ω value contour

A certain y-section slice located at $x = 439.8$ with Ω value and spanwise velocity v contours are shown in Figure 7-11, 12 and 13. Figure 7-11 gives the distribution of Ω value on this slice, highest Ω values at about 0.65 are obtained inside the leg-like vortices. Figure 7-12 verifies Liu's theory that high Ω value region presents the core of rotation. The reason is the existence of the rotational streamline on high Ω region. In Figure 7-13, distribution of v velocity provides a typical rotation flow profile.

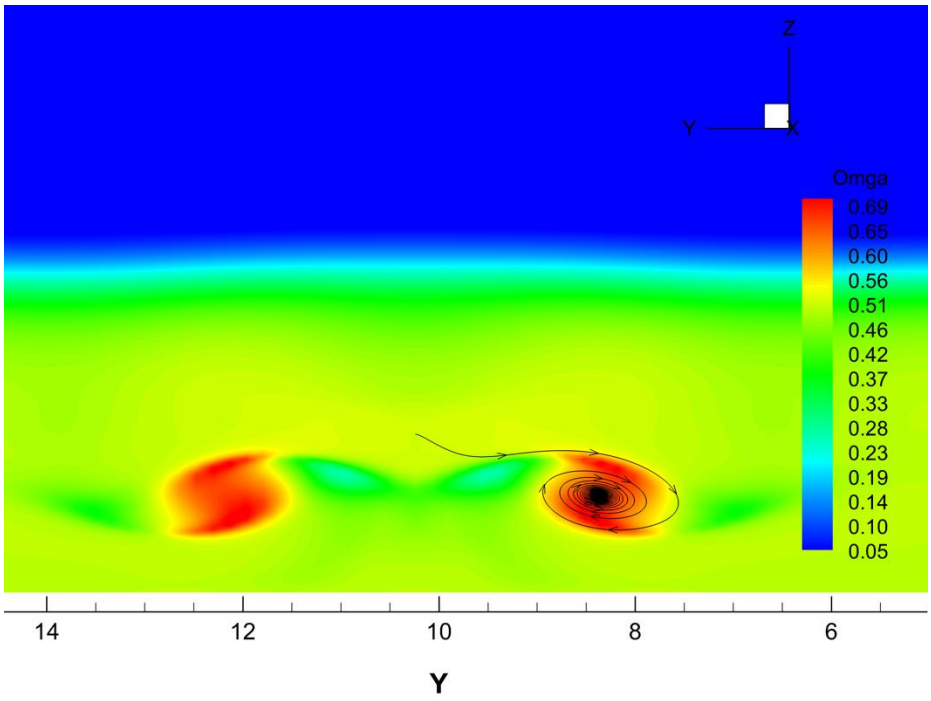

Figure 7-12 y-section slice at $x = 439.8$, Ω value contour with a streamline

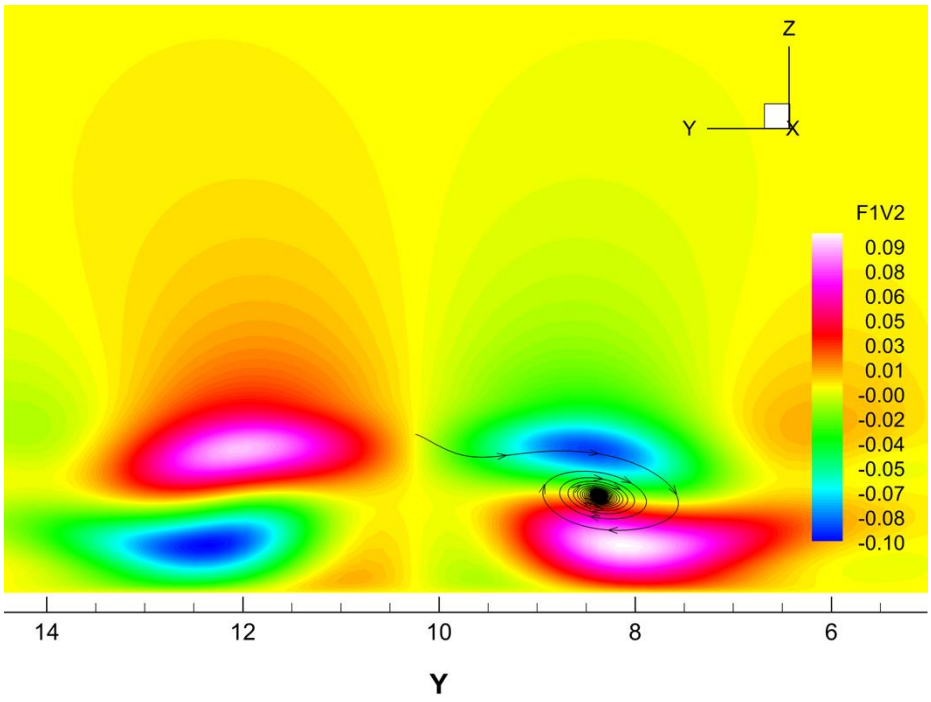

Figure 7-13 y-section slice at $x = 439.8$, v value contour with a streamline

7.2.2 Numerical results

Extracted spanwise v velocity profiles from slices S1, S2 and S3 shown in Figure 7-10, apply them as the quasi-rotational base flow to solve Equation (6.41) by using Quadratic Shifted Chebyshev polynomials associated with collocation points (Chebyshev nodes).

The Reynolds number Re=1000 in DNS case, given $\alpha = 1$, $N = 100$ and $M = 200$. N is the order of Shifted Chebyshev polynomials, M is the number of collocation points.

Three base flow velocity profiles related to S1, S2 and S3 are shown in Figure 7-14. The least stable imaginary eigenvalues c_i for three cases are given in Table 7-2. Spectrum distributions are depicted in Figure 7-15. Figure 7-16 shows the eigenfunction $\hat{u}$ of these unstable modes.

Table 7-2 also provides the Ω values of each core of vortex, largest Ω value connected with smallest positive imaginary eigenvalue, and smallest Ω with the largest positive. However, three cases are not enough to show the relationship between Ω value and stability. To study the stability of leg-like vortex deeply, Figure 7-17 is presented, the Ω values and least stable c_i are obtained by tracking a vortex over time. The result shows that with the Ω increasing over time, the vortex trends to be more stable with the decrement of the positive imaginary part of eigenvalues.

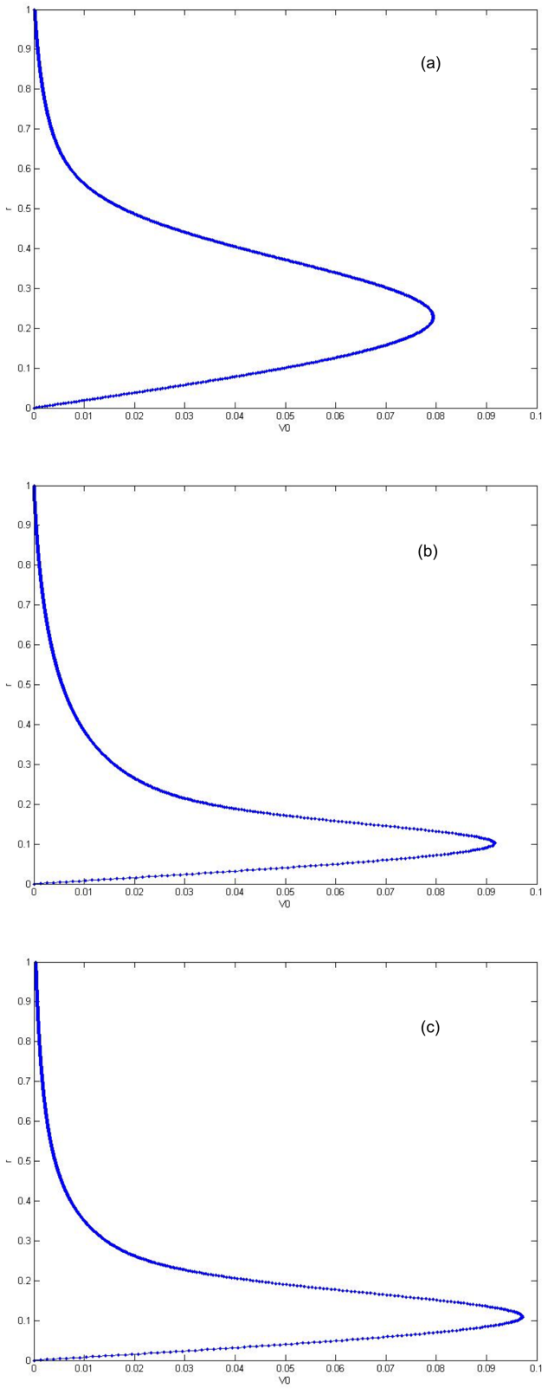

Figure 7-14 velocity profiles from (a) s1; (b) s2; (c) s3

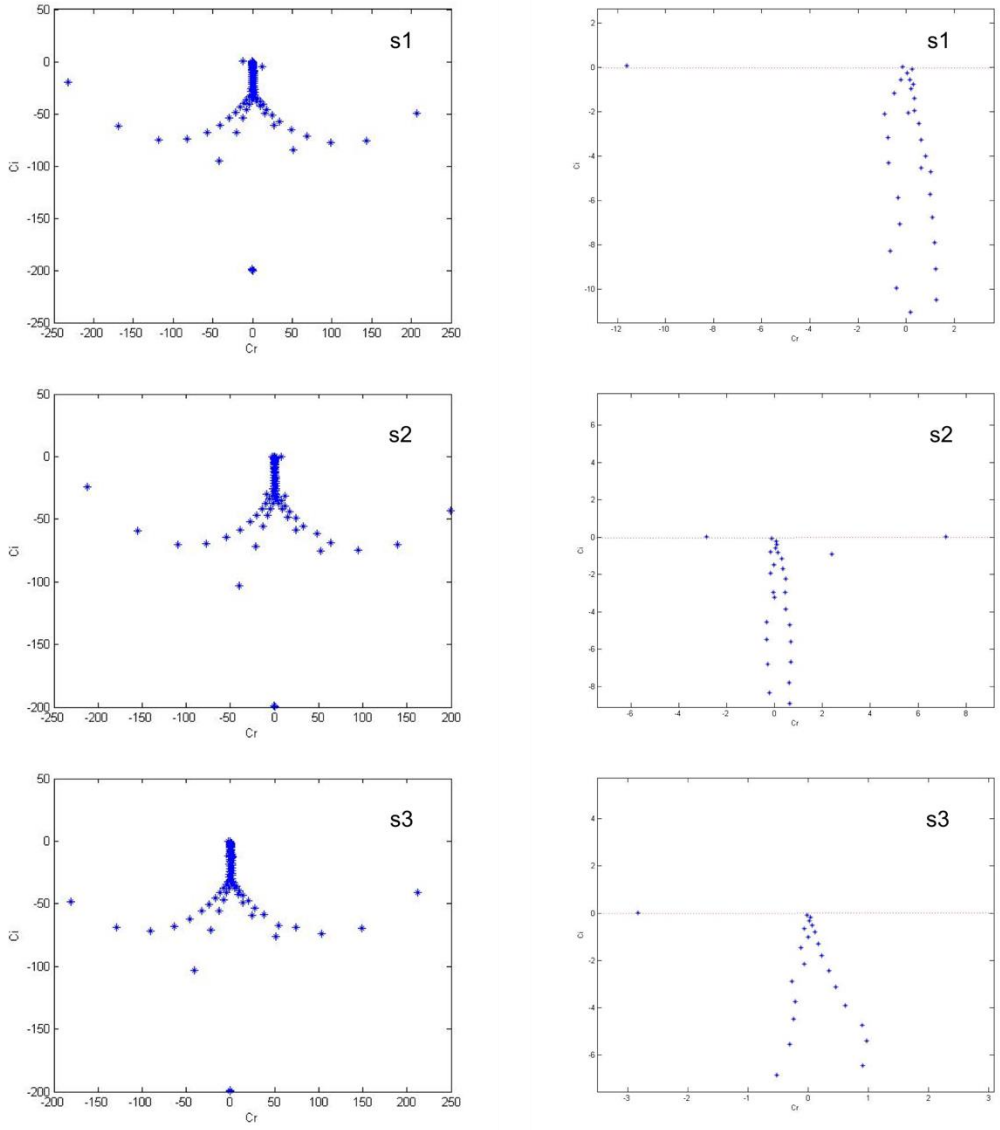

(a) global view (b) zoom-in view

Figure 7-15 Distribution of spectrums on three base flows

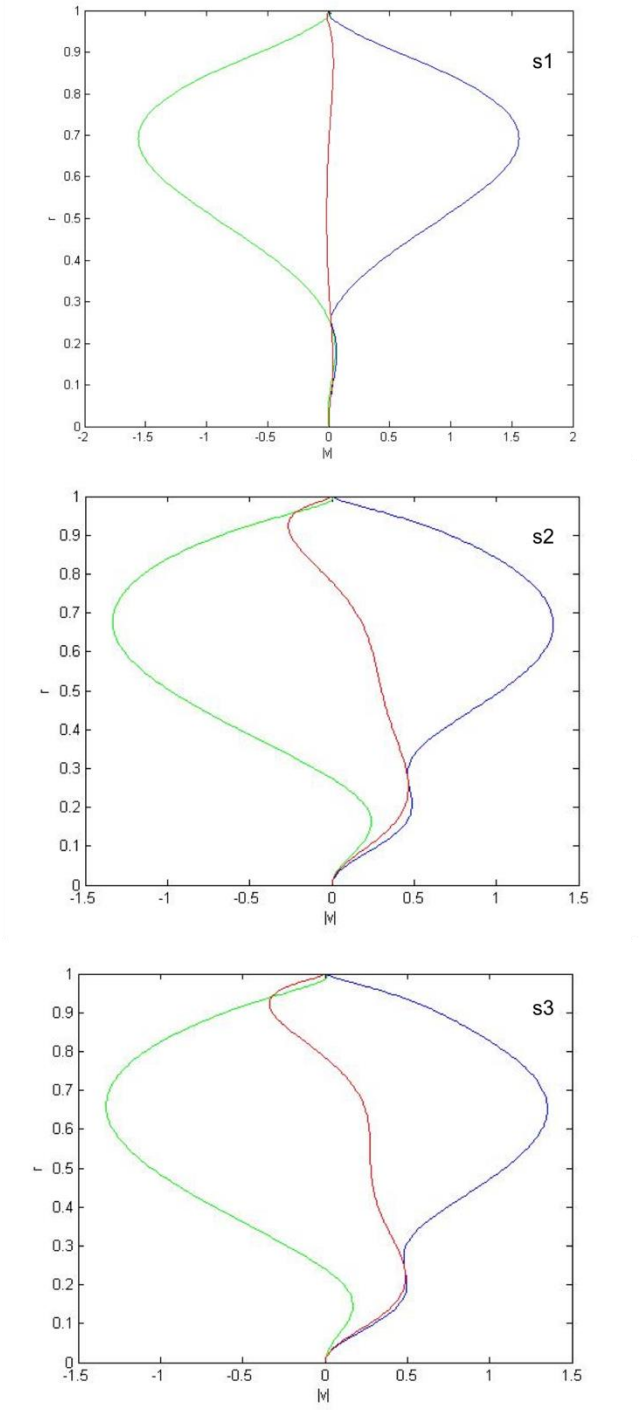

Figure 7-16 Eigenfunction $\hat{u}$ on three base flows

Table 7-2 Most unstable eigenvalues related with Omega value

Slices	c_i	Ω
1	0.0303338	0.632872
2	0.0161457	0.662620
3	0.0148870	0.668555

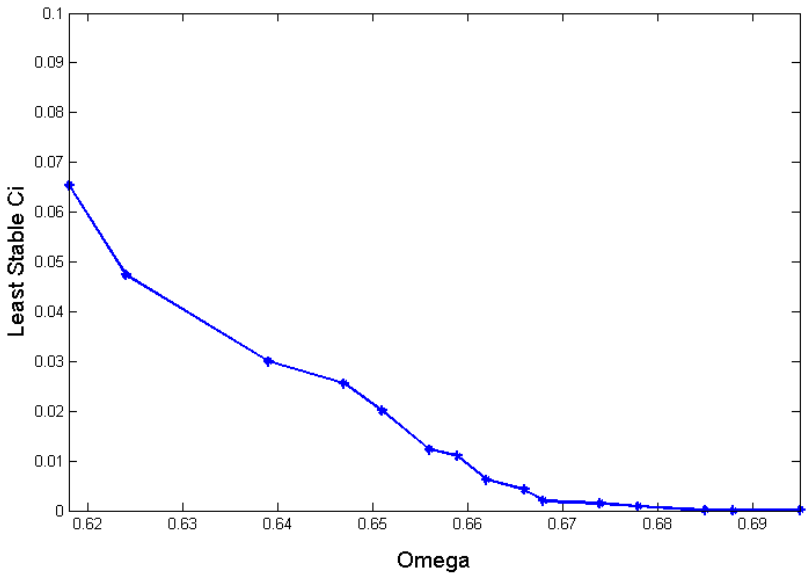

Figure 7-17 least stable c_i vs Ω value on leg-like vortex

7.3 DNS ring-like vortices cases

7.3.1 DNS observations

Ring-like vortices are generated at the head of the leg-like vortices (see Figure 7-17). Similar with leg-like vortices, high shear stress locates the same region before ring-like vortices appear. Figure 7-18,19 provides some illustrations of u velocity and shear layers in certain regions.

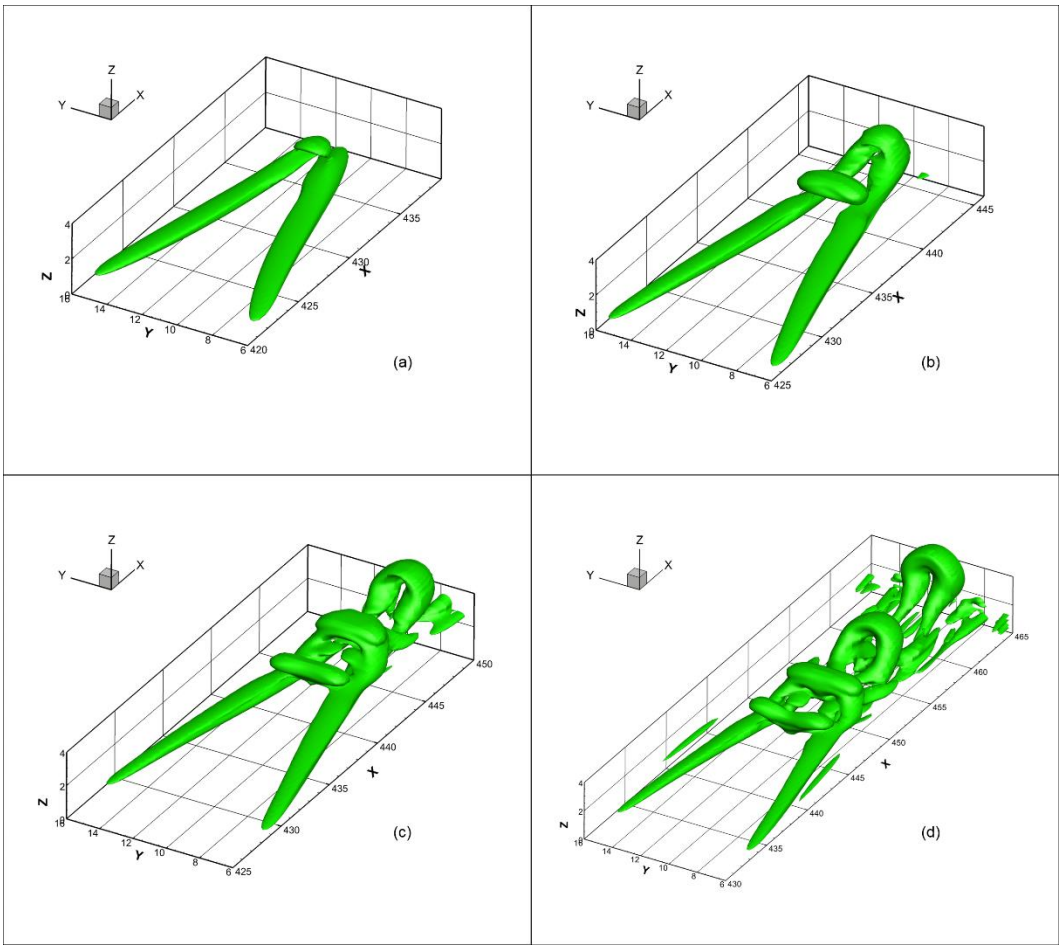

Figure 7-18 Generation of ring-like vortex at (a) t=6.30T; (b) t= 6.52T; (c) t=6.66T; (d) t=6.87T

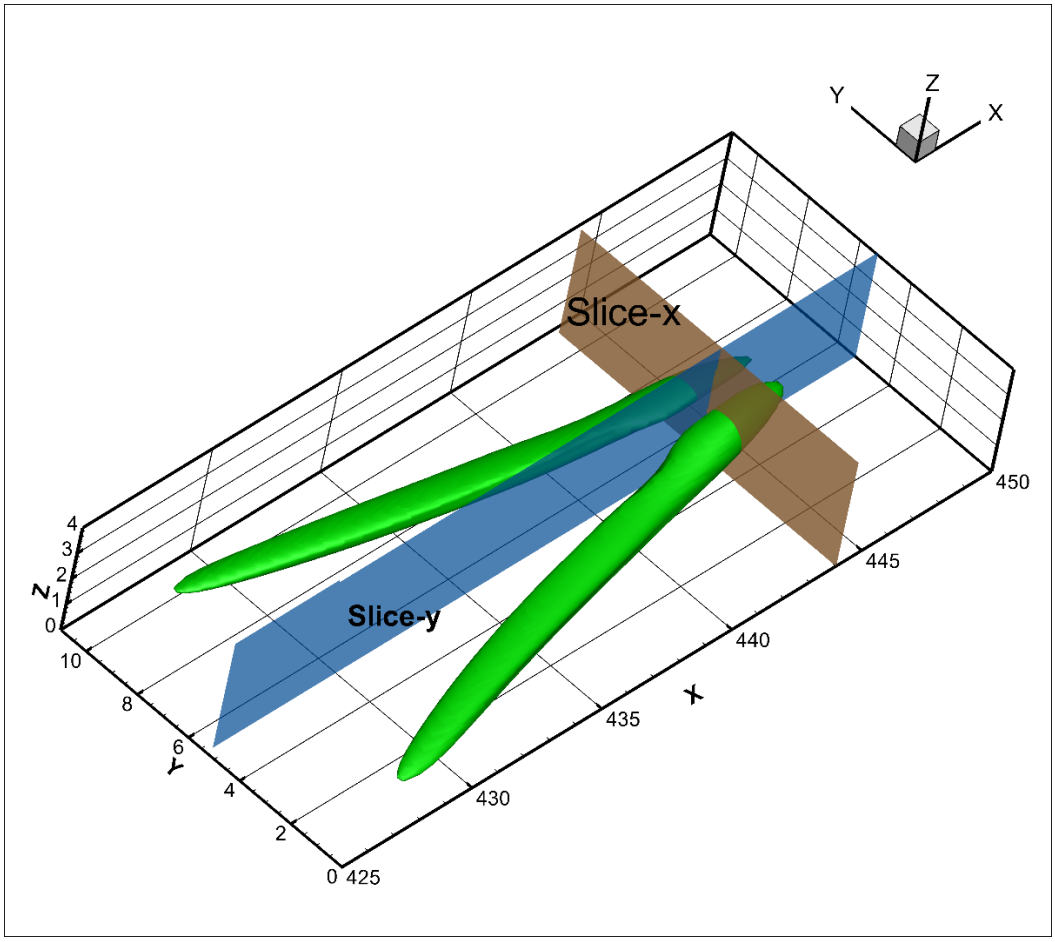

Figure 7-19 Illustrations of Slice-x and y locations on DNS flow field

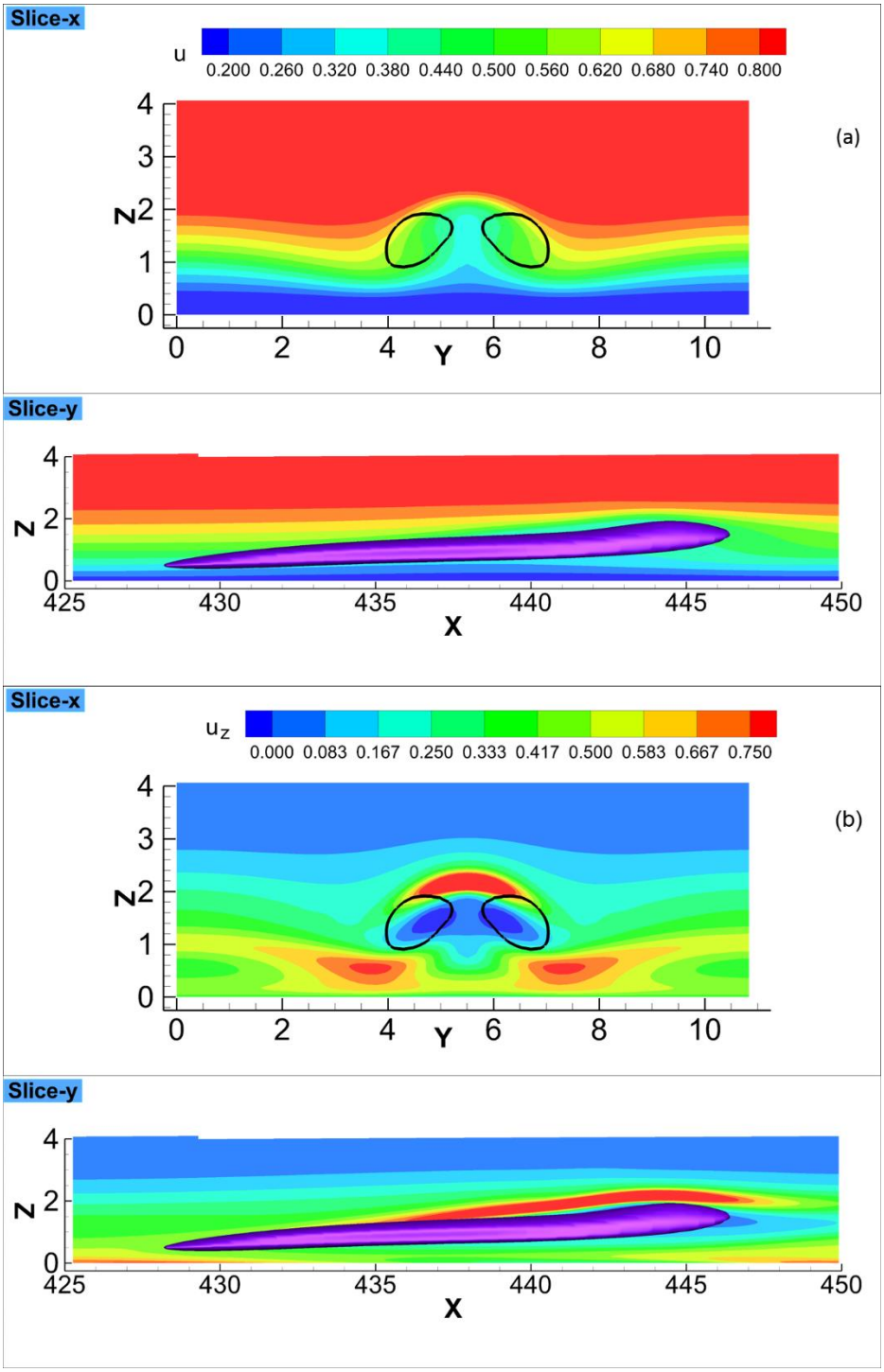

Figure 7-20 Distribution of u velocity and gradient in z direction

7.3.2 Numerical results

The technique used to solve ring-like vortices problems is same with leg-like vortices. Figure 7-21 gives the section of ring-like vortices along with streamwise direction at $t = 10.914$. Figure 7-22 shows the Ω distribution on the certain slice. The velocity profile of the given slice is shown in Figure 7-23. The numerical results under this base flow, is provide in Figure 7-24 and 7-25, showing the eigenvalues and eigenfunctions respectively.

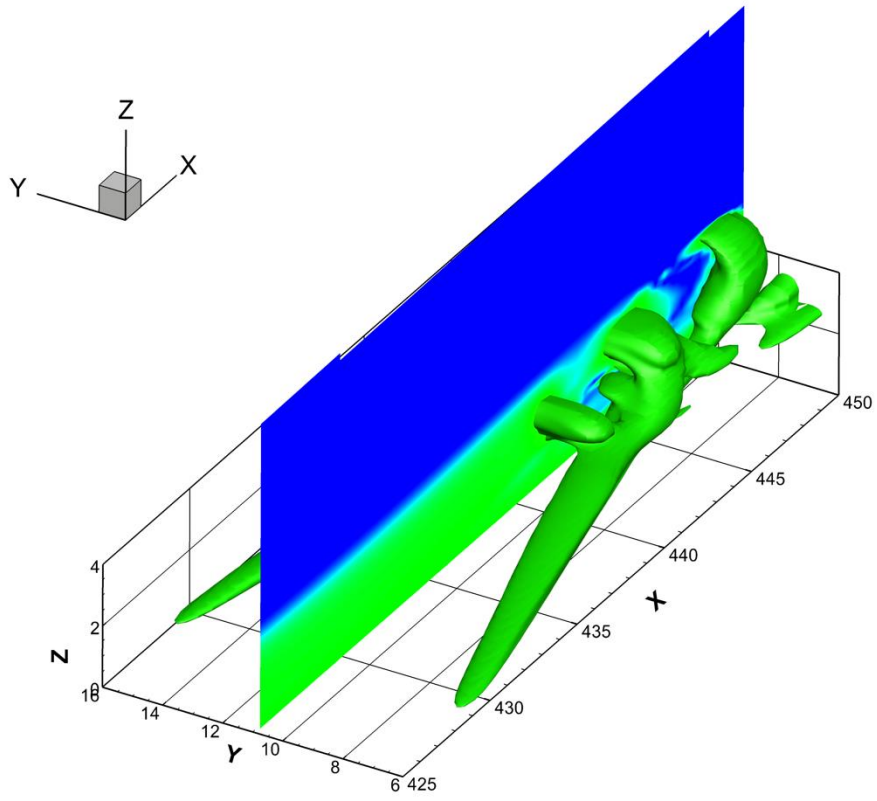

Figure 7-21 Section of ring-like vortices at $y = 10.914$ on $t = 6.66T$

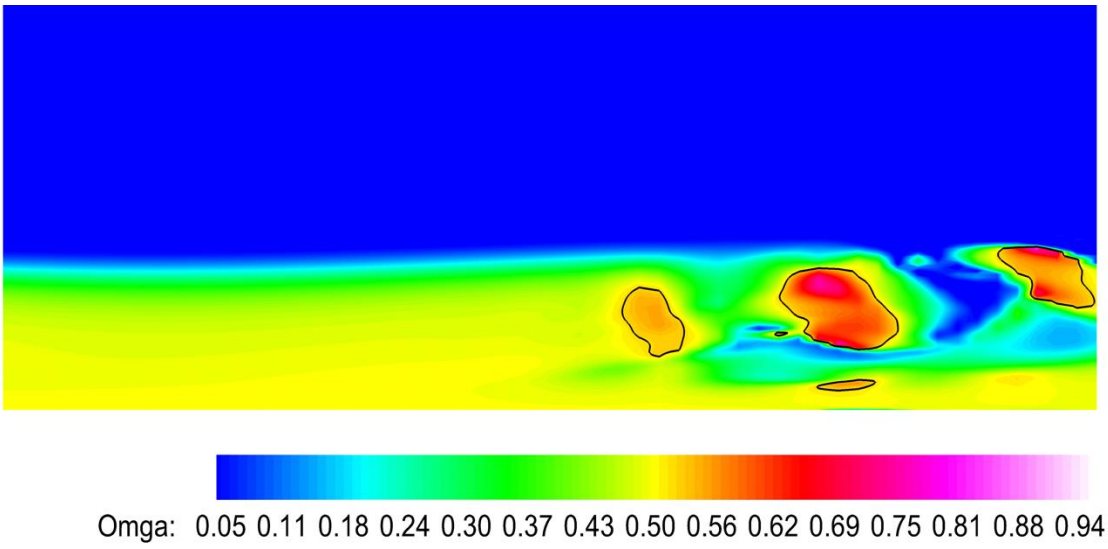

Figure 7-22 Distribution of Ω value with three rings

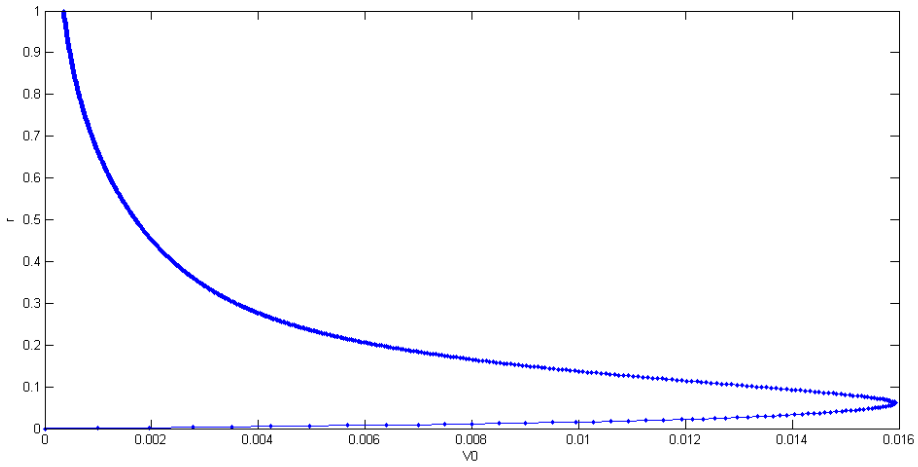

Figure 7-23 Velocity Profile on the certain slice at $t = 6.66T$

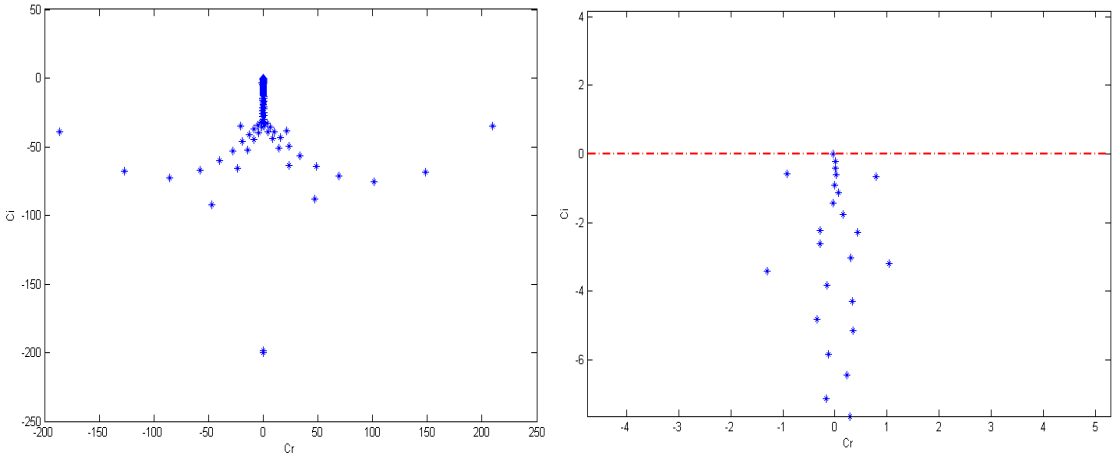

(a) global view (b) zoom-in view

Figure 7-24 Eigenvalues distribution with unstable $c_i = 0.0095$

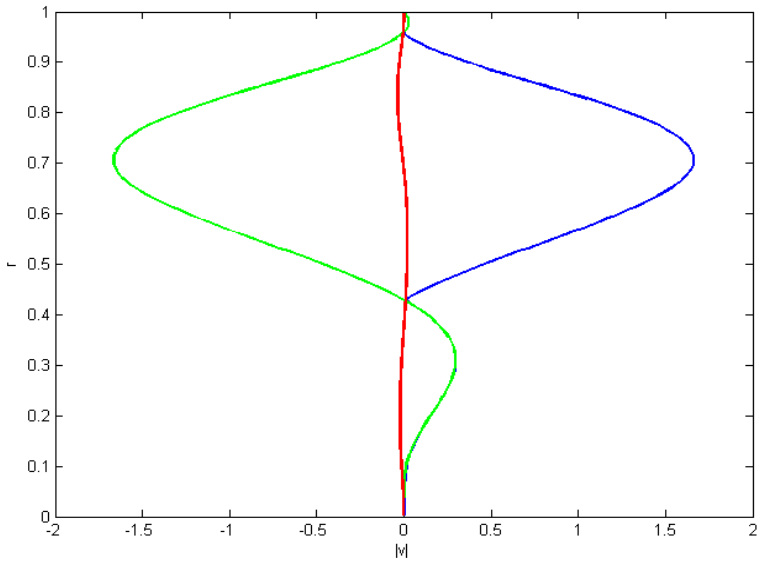

Figure 7-25 Eigenfunction $\hat{u}$ with $c_i = 0.0095$

By tracking a fixed streamwise ring-like vortex from $t = 6.59T$ to $6.87T$, the relationship between imaginary part of the eigenvalue with respect to the least stable mode and the Ω value on the core of vortex over time is shown on Figure 7-26. It clearly describes that the vortex trends to be more stable as the Ω increased over time.

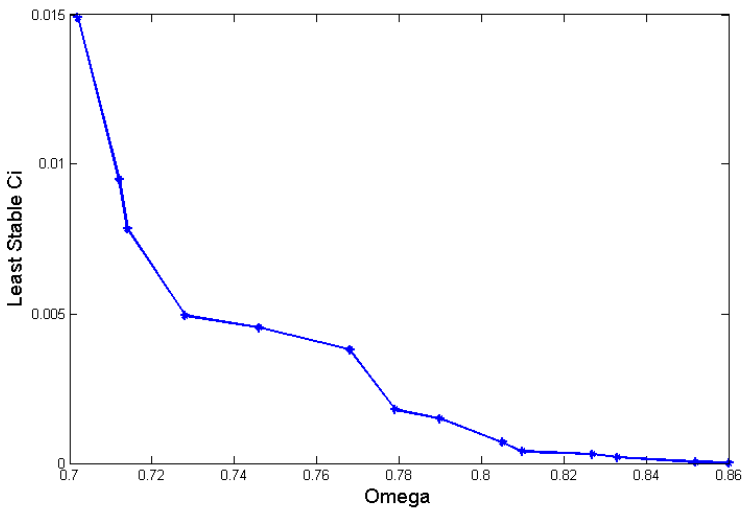

Figure 7-26 least stable c_i vs Ω value on ring-like vortex

7.4 Conclusion

1. Chebyshev collocation method associated with Quadratic Shifted Chebyshev polynomials performs well in solving the fourth order ODE, the linear stability equation for symmetric flow we derived in Chapter 7.
2. Linear Shifted Chebyshev polynomials are invalid in interpolating certain equation. The clustering points near the singular point $r = 0$ in Cylindrical Coordinate might be dangerous in convergence.
3. The linear stability equation for symmetric flow can be used to analyze the stability of real-case quasi-rotation flow obtained from our DNS data. The result shows that, in the flow transition process, new vortices including vortex legs and vortex rings, the Omega becomes larger and the vortex become less unstable in the fact of decreasing positive eigenvalues. When the Omega of vortex becomes larger, the flow become more stable (or less unstable).
4. Dr. Liu's theory that turbulent flow which is dominated by rotations is more stable than laminar flow which is dominated by shears has been numerically checked and verified to be correct.

References

[1] G. K. Batchelor, “An Introduction to Fluid Dynamics,” *Book*. p. 631, 1967.

[2] C. J. Geankoplis, “Transport Processes and Separation Process Principles: Includes Unit Operations,” in *Transport Processes and Separation Process Principles (Includes Unit Operations)*, 2003, p. 1026.

[3] R. Nave, “Laminar Flow.” [Online]. Available: http://hyperphysics.phy-astr.gsu.edu/hbase/pfric.html.

[4] I. Tani, “Boundary-Layer Transition,” *Annu. Rev. Fluid Mech.*, vol. 1, pp. 169–196, 1969.

[5] Y. S.Kachanov, “Physical mechanisms of laminar-boundary-layer transition,” *Annu. Rev. Fluid Mech.*, vol. 26, pp. 411–482, 1994.

[6] V. M. Epifanov, “Boundary Layer.” .

[7] L. Prandtl, “Motion of Fluids with Very Little Viscosity,” *Int. Math.*, pp. 1–8, 1904.

[8] W. S. Saric, H. L. Reed, and E. J. Kerschen, “Boundary-Layer Receptivity to Freestream Disturbances,” *Annu. Rev. Fluid Mech.*, vol. 34, no. 1, pp. 291–319, 2002.

[9] L. M. Mack, “Boundary-Layer Linear Stability Theory,” in *AGARD Special Course on Stability and Transition of Laminar Flow*, 1984, pp. 1–81.

[10] M. V Morkovin and W. Patterson, “Critical evaluation of transition from laminar to turbulent shear layer with emphasis on hypersonically traveling bodies,” 1969.

[11] M. V. Morkovin, “Bypass transition to turbulence and research desiderata,” *NASA CP-2386 Transit. Turbines*, pp. 161–204, 1985.

[12] M. V. Morkovin and E. Reshotko, “Dialogue on progress and issues in stability and transition research,” in *Laminar–Turbulent Transition: IUTAM Symposium, Toulouse/France, September 11–15, 1989*, 1990, pp. 3–29.

[13] R. I. Loehrke, M. V. Morkovin, and A. A. Fejer, “Review — Transition in nonreversing oscillating boundary layers,” *J. Fluids Eng.*, vol. 97, no. 4, pp. 534–549, 1975.

[14] E. Reshotko, “Boundary-Layer Stability and Transition,” *Annu. Rev. Fluid Mech.*, vol. 8, no. 1, pp. 311–349, 1976.

[15] V. P. Maksimov, “Origin of Tollmien–Schlichting waves in oscillating boundary layers,” in *Development of Disturbances in Boundary Layer*, 1979, pp. 68–75.

[16] Y. S. K. V. K. Y. L. P. Maksimov, “The transformation of external disturbances into the boundary layer waves,” in *Sixth International Conference on Numerical Methods in Fluid Dynamics*, 1979, pp. 299–307.

[17] A. M. Zhigulyov, V. N.;Tumin, “Onset of turbulence. Dynamical theory of excitation and development of instabilities in boundary layers,” *Novosibrisk, Sib*, p. 282, 1987.

[18] M. Nishioka and M. Morkovin, “Boundary-layer receptivity to unsteady pressure gradients: experiments and overview,” *J. Fluid Mech.*, vol. 171, pp. 219–261, 1986.

[19] M. E. Goldstein and L. S. Hultgren, “Boundary-Layer Receptivity to Long-Wave Free-Stream Disturbances,” *Annu. Rev. Fluid Mech.*, vol. 21, no. 1, pp. 137–166, 1989.

[20] R. A. E. Heinrich and E. J. Kerschen, “Leading-edge boundary layer receptivity to various free-stream disturbance structures,” *Zeitschrift für Angew. Math. und Mech.*, vol. 69, no. 6, pp. T596–T598, 1989.

[21] E. J. Kerschen, “Boundary Layer Receptivity Theory,” *Appl. Mech. Rev.*, vol. 43, no. 5S, p. S152, 1990.

[22] W. Tollmien, “Ueber die Entstehung der Turbulenz - The production of

turbulence," 1929.

[23] D. H. Schlichting and K. Gersten, "Boundary-layer theory," *Eur. J. Mech. - B/Fluids*, vol. 20, p. 817, 1979.

[24] S. C. Lin, E. L. Resler, and A. Kantrowitz, "Electrical conductivity of highly ionized argon produced by shock waves," *J. Appl. Phys.*, vol. 26, no. 1, pp. 95–109, 1955.

[25] T. Herbert, "On finite amplitudes of periodic disturbances of the boundary layer along a flat plate," in *Proceedings of the Fourth International Conference on Numerical Methods in Fluid Dynamics*, 1975.

[26] L. Kleiser and T. a. Zang, "Numerical simulation of transition in wall-bounded shear flows," *Annu. Rev. Fluid Mech.*, vol. 23, no. 1, pp. 495–537, 1991.

[27] N. D. Sandham and L. Kleiser, "The late stages of transition to turbulence in channel flow," *J. Fluid Mech.*, vol. 245, pp. 319–348, 1992.

[28] U. Rist and Y. S. Kachanov, "Numerical and experimental investigation of the K-regime of boundary-layer transition," in *Laminar–Turbulent Transition: IUTAM Symposium, Sendai/Japan, September 5–9, 1994*, 1995, pp. 405–412.

[29] S. Bake, D. G. W. Meyer, and U. Rist, "Turbulence mechanism in Klebanoff transition: a quantitative comparison of experiment and direct numerical simulation," *J. Fluid Mech.*, vol. 459, pp. 217–243, 2002.

[30] V. I. Borodulin, V. R. Gaponenko, Y. S. Kachanov, D. G. W. Meyer, U. Rist, Q. X. Lian, and C. B. Lee, "Late-stage transitional boundary-layer structures. Direct numerical simulation and experiment," *Theor. Comput. Fluid Dyn.*, vol. 15, no. 5, pp. 317–337, 2002.

[31] Y. S. Kachanov, "On a Universal Mechanism of Turbulence Production in Wall Shear Flows," in *Recent Results in Laminar-Turbulent Transition*, 2004, pp. 4–5.

[32] C. Liu, Y. Yan, and P. Lu, "Physics of turbulence generation and sustenance in a

boundary layer," *Comput. Fluids*, vol. 102, pp. 353–384, 2014.

[33] C. Chen, Lin; Liu, "Vortical structure, sweep and ejection events in transitional boundary layer," *Sci. China, Ser. G, Physics, Mech. Astron.*, vol. 39, no. 10, pp. 1520–1526, 2009.

[34] X. Liu and L. Chen, "DNS for Ring - Like Vortices Formation and Roles in," in *48th AIAA Aerospace Sciences Meeting*, 2010, no. January, p. 1471.

[35] C. Chen, Lin ; Tang, Dengbin; Lu, Ping; Liu, "Evolution of the vortex structures and turbulent spots at the late-stage of transitional boundary layers," *Sci. China Physics, Mech. Astron.*, vol. 54, no. 5, pp. 986–990, 2011.

[36] L. Chen and C. Liu, "Numerical study on mechanisms of second sweep and positive spikes in transitional flow on a flat plate," *Comput. Fluids*, vol. 40, no. 1, pp. 28–41, 2011.

[37] C. Liu and L. Chen, "Study of Mechanism of Ring-Like Vortex Formation in Late Flow Transition," in *AIAA Aerospace Sciences Meeting*, 2010, vol. 1456, no. January, pp. 1–21.

[38] L. Chen, X. Liu, M. Oliveira, and C. Liu, "DNS for Late Stage Structure of Flow Transition on a Flat-Plate Boundary Layer," *AIAA Pap.*, vol. 2010–1470, no. January, pp. 19408–19408, 2010.

[39] C. Liu, L. Chen, and P. Lu, "New findings by high-order DNS for late flow transition in a boundary layer," *Model. Simul. Eng.*, vol. 2011, 2011.

[40] C. Liu and L. Chen, "Parallel DNS for vortex structure of late stages of flow transition," *Comput. Fluids*, vol. 45, no. 1, pp. 129–137, 2011.

[41] C. Liu, "Numerical and theoretical study on 'vortex breakdown,'" *Int. J. Comput. Math.*, vol. 88, no. 17, pp. 3702–3708, 2011.

[42] C. Liu, L. Chen, P. Lu, and X. Liu, "Study on multiple ring-like vortex formation and

small vortex generation in late flow transition on a flat plate," *Theor. Comput. Fluid Dyn.*, vol. 27, no. 1–2, pp. 41–70, 2013.

[43] C. Lu, Ping;Li, Qing;Liu, "Numerical Study of Mechanism of U-shaped Vortex Formation," in *49th AIAA Aerospace Sciences Meeting*, 2011, p. 286.

[44] C. Liu and L. Zhining, "Multigrid mapping and box relaxation for simulation of the whole process of flow transition in 3D boundary layers," *J. Comput. Phys.*, vol. 119, no. 2, pp. 325–341, 1995.

[45] C. Liu, zhining;Xiong, Guohua;Liu, "Direct numerical simulation for the whole process of transition on 3-D airfoils," in *27th AIAA Fluid Dynamics Conference*, 1996, p. 2081.

[46] C. Z. Liu, "Direct Numerical Simulation for Flow Transition Around Airfoils," 1997.

[47] P. Lu, Z. Wang, L. Chen, and C. Liu, "Numerical study on U-shaped vortex formation in late boundary layer transition," *Comput. Fluids*, vol. 55, no. January, pp. 36–47, 2012.

[48] C. Yan, Yonghua;Liu, "Shear layer stability analysis in later boundary layer transition and MVG controlled flow," in *51st AIAA Aerospace Sciences Meeting*, 2013, p. 531.

[49] Y. Yan, C. Chen, H. Fu, and C. Liu, "DNS study on $Δ$-vortex and vortex ring formation in flow transition at Mach number 0.5," *J. Turb.*, vol. 15, no. 1, pp. 1–21, 2014.

[50] C. Wang, Yiqian;Yang, Yong;Yang, Guang;Liu, "DNS Study on Vortex and Vorticity in Late Boundary Layer Transition," *Commun. Comput. Phys.*, vol. 22, no. 2, pp. 441–459.

[51] X. Liu, Chaoqun;Cai, "New theory on turbulence generation and structure—DNS and experiment," *Sci. CHINA Physics, Mech. Astron.*, vol. 60, no. 8, 2017.

[52] G. G. Stokes, *On the effect of the internal friction of fluids on the motion of pendulums*. Transactions of the Cambridge Philosophical Society, 1851.

[53] T. A. Canuto, C.;Hussaini, M.Y.;Quarteroni, A.;Zang, *Spectral Methods in Fluid Dynamics*. Springer Science & Business Media, 1988.

[54] R. Peyret, “Chebyshev method,” in *Spectral methods for incompressible viscous flow*, Springer Science & Business Media, 2013, p. 39.

[55] S. A. Orszag, “Accurate solution of the Orr-Sommerfeld stability equation,” *J . Fluid Mech*, vol. 50, no. 4, pp. 659–703, 1971.

[56] S. K. Lele, “Compact finite difference schemes with spectral-like resolution,” *J. Comput. Phys.*, vol. 103, no. 1, pp. 16–42, 1992.

[57] C. jiang, Li;Chang, Chau-Lyan;Choudhari, Meelan;Liu, “Cross-Validation of DNS and PSE Results for Instability-Wave Propagation in Compressible Boundary Layers past Curvilinear Surfaces,” in *16th AIAA Computational Fluid Dynamics Conference*, 2003.

[58] J. Jeong and F. Hussain, “On the identification of a vortex,” *J. Fluid Mech.*, vol. 285, no. February, pp. 69–94, 1995.

[59] C. Lee and R. Li, “Dominant structure for turbulent production in a transitional boundary layer,” *J. Turbul.*, vol. 8, no. 55, p. N55, 2007.

[60] Z. Liu, Chaoqun;Wang, yiqian;Yang, Yong;Duan, “New omega vortex identification method,” *Sci. China Physics, Mech. Astron.*, vol. 59, no. 684711, 2016.

Biographical Information

Jie Tang was born in Yancheng, Jiangsu, China, in 1989. She received her B.S. degree from North China University of Technology in 2011, her Ph.D. degree from The University of Texas at Arlington in Applied Mathematics, in 2017. During her five years doctoral studies, she also served as a Graduate Teaching Assistant in the department of mathematics. She received The R. Kannan Memorial Scholarship Award in 2016.